Steel and Composite Structures, *Vol. 36, No. 2 (2020) 143-161*
DOI: https://doi.org/10.12989/scs.2020.36.2.143

Bending behavior of squared cutout nanobeams incorporating surface stress effects

Mohamed A Eltaher*[1,2] and Alaa A. Abdelrahman[2a]

[1]*Mechanical Engineering Department, Faculty of Engineering, King Abdulaziz University, P.O. Box 80204, Jeddah, Saudi Arabia*
[2]*Mechanical Design & Production Department, Faculty of Engineering, Zagazig University, P.O. Box 44519, Zagazig, Egypt*

(*Received May 3, 2020, Revised June 28, 2020, Accepted June 30, 2020*)

Abstract. In nanosized structures as the surface area to the bulk volume ratio increases the classical continuum mechanics approaches fails to investigate the mechanical behavior of such structures. In perforated nanobeam structures, more decrease in the bulk volume is obtained due to perforation process thus nonclassical continuum approaches should be employed for reliable investigation of the mechanical behavior these structures. This article introduces an analytical methodology to investigate the size dependent, surface energy, and perforation impacts on the nonclassical bending behavior of regularly squared cutout nanobeam structures for the first time. To do this, geometrical model for both bulk and surface characteristics is developed for regularly squared perforated nanobeams. Based on the proposed geometrical model, the nonclassical Gurtin-Murdoch surface elasticity model is adopted and modified to incorporate the surface energy effects in perforated nanobeams. To investigate the effect of shear deformation associated with cutout process, both Euler-Bernoulli and Timoshenko beams theories are developed. Mathematical model for perforated nanobeam structure including surface energy effects are derived in comprehensive procedure and nonclassical boundary conditions are presented. Closed forms for the nonclassical bending and rotational displacements are derived for both theories considering all classical and nonclassical kinematics and kinetics boundary conditions. Additionally, both uniformly distributed and concentrated loads are considered. The developed methodology is verified and compared with the available results and an excellent agreement is noticed. Both classical and nonclassical bending profiles for both thin and thick perforated nanobeams are investigated. Numerical results are obtained to illustrate effects of beam filling ratio, the number of hole rows through the cross section, surface material characteristics, beam slenderness ratio as well as the boundary and loading conditions on the non-classical bending behavior of perforated nanobeams in the presence of surface effects. It is found that, the surface residual stress has more significant effect on the bending deflection compared with the corresponding effect of the surface elasticity, Es. The obtained results are supportive for the design, analysis and manufacturing of perforated nanobeams.

Keywords: surface stress effects; squared cutout nanobeams; filling ratio; shear deformation; nonclassical bending; closed forms

1. Introduction

Perforated materials are a reliable method which can be applied in many practical applications in modern society and industrial applications. Perforation is a very common procedure in MEMS fabrication. The release of beams and plates is often obtained by sacrificial etching through a pattern of holes fabricated on these structures. Perforations, though introduced for a technological reason, affect the behavior of MEMS structures in various ways. However, their effect on the mechanical behavior of beams and plates has been extensively investigated only for specific cases and applications, Luschi and Pieri (2014).

Elements structure such as, beams, plates and shells are widely used in real applications, ranging from macro-scale applications (i.e., aerospace, civil, mechanical and nuclear structures), to micro-scale applications (i.e., actuators, resonators, switches, and RF MEMS), and to nano-scale applications (i.e., AFM, nanoprobes, nanoactuators, and nanoswitches), Abdelrahman *et al*. (2019). Nowadays, perforation is a geometric procedure widely used in advanced technologies to develop sensitive structures such as in the heat exchangers and nuclear power plants applications (Jeong and Amabili 2006), in ships and offshore structures Kim *et al*. (2015), and in optomechanics and photonics Chan *et al*. (2009).

As a macro-scale structure, Luschi and Pieri (2012) introduced closed forms for equivalent bending stiffness in the filled and the perforated sections of perforated beam to examine bending properties of beams with regular rectangular perforations. Xiao *et al.* (2012) exploited wave expansion method to study the flexural wave propagation in locally resonant beams with multiple periodic arrays of attached spring-mass resonator. Sun *et al*. (2017) carried out experiments to reveal cutout effects on stress concentrations, failure styles, natural frequencies and mode shapes of conical carbon fiber reinforced composite lattice-core sandwich cylinder. Sivakumar *et al.* (2018)

*Corresponding author, Professor
E-mail: meltaher@kau.edu.sa
[a]Professor
E-mail: alaaabouahmed@gmail.com

http://www.techno-press.org/?journal=scs&subpage=8 ISSN: 1229-9367 (Print), 1598-6233 (Online)

investigated 3D static bending of a perforated beam due to applied loading and electrostatic forces together. Choudhary *et al.* (2019) exploited global optimization Genetic Algorithm tool to optimize the location of cutout within laminated cantilever beam for maximum lateral buckling load. Chaabane *et al.* (2019) studied analytically bending and free vibration responses of FG beams resting on elastic foundation. Zhang *et al.* (2019) presented mixed experimental-numerical analysis to simulate modal characteristics of micro-perforated sandwich beams with square honeycomb-corrugation hybrid cores. Abdelrahman *et al*. (2019) and Almitani *et al.* (2019) studied the free and forced vibration of perforated beam with regular array of squares by using analytical method and derived closed forms for resonant frequencies, corresponding Eigen-mode functions. Ansari *et al.* (2019, 2020) studied buckling and vibration of functionally graded (FG) carbon nanotube-reinforced composite plates with the arbitrarily shaped cutout using a numerical approach.

In a nanoscale system, the dimensions of the structures are akin to their inter-atomic distances, which means that classical continuum models are incapable to incorporate size-scale effects in the solution, Eltaher *et al*. (2013a). So, modified continuum models such as micromorphic, micropolar theory, Cosserat theory, nonlocal elasticity theory, couple stress theory and surface energy effects have been proposed to include micro/nano-scale effects and encompass classical continuum mechanics at macroscale, Eltaher *et al*. (2014a). Ansari and Sahmani (2011) studied bending and buckling behaviors of nanobeams including surface stress effects corresponding to different beam theories. Mahmoud *et al.* (2012) and Eltaher *et al.* (2013a) studied the coupled effects of surface energy properties and nonlocal elasticity on static and vibration of nanobeams by using finite element method. Khater *et al*. (2014) examined impact of surface energy and thermal loading on the static stability of curved nanowire. Eltaher *et al*. (2016) exploited two scale size dependent model including material scale and size-scale to investigate the nonlinear bending of nonlocal nanobeam. Agwa and Eltaher (2016) investigated the influence of surface elasticity and residual surface tension on the natural frequency of nanomechanical mass sensor using a carbyne resonator. Ebrahimi *et al*. (2017) presented influenced surface energy on vibration and buckling behavior of embedded nanoarches. Phung-Van (2017a, b) developed nonlinear transient isogeometric analysis of smart piezoelectric FG plates under thermo-electro-mechanical loads. Bellifa *et al.* (2017) developed a nonlocal zeroth-order shear deformation theory to study nonlinear postbuckling of nanobeams. Ebrahimi and Barati (2018) studied surface and flexoelectricity effects on size-dependent thermal stability of smart piezoelectric nanoplates. Ebrahimi and Barati (2018) investigated stability of porous multi-phase nanocrystalline nonlocal beams based on a general higher-order couple-stress beam model. Li *et al*. (2018) developed nonlocal strain gradient beam model incorporating the thickness effect in buckling analysis of nanobeams, and derived closed-form solutions for post-buckling configuration and critical buckling force. Phung-Van *et al*. (2018) and Thanh *et al.* (2018, 2019a) investigated nonlinear transient isogeometric analysis of FG-CNTRC damped and undamped nanoplates in thermal environments. Ebrahimi *et al.* (2019a, b) and Vinyas (2020) and Vinyas *et al.* (2019a, b) studied frequency response of porous FG magneto-electro-elastic plates and beams. Ebrahimi *et al*. (2019c, d, e) studied scale-dependent vibration behavior of flexoelectric nanobeams by using surface energy and nonlocal strain gradient elasticity theories. Based on finite element method, Vinyas and Kattimani (2017a, b, c, d) investigated the elastostatic behavior the coupled magneto-electro-elastic smart beams and plate structures under different mechanical or thermomechanical loading conditions. Extensions of these works to study the vibration behavior of these smart structures have been developed by Mahesh *et al.* (2018); Vinyas and Kattimani (2018a, b), Vinyas *et al*. (2018a, b). Eltaher *et al*. (2019a) illustrated coupled effects of nonlocal elasticity and surface properties on static and vibration characteristics of piezoelectric nanobeams using thin beam theory and finite element method. Karimiasl *et al.* (2019a, b) investigated postbuckling and nonlinear vibration of piezoelectric multiscale sandwich composite doubly curved porous shallow shells. The frequency response and the coupled evaluation of the vibrations characteristics as well as the damping effect on the coupled vibration response were investigated and analyzed by Mahesh and Kattimani (2019), Mahesh *et al*. (2019) and Vinyas *et al*. (2019). Comprehensive review and dynamic investigations of functionally graded smart structures have been reported in Vinyas (2020a, b) and Vinyas *et al*. (2020a, b). Benahmed *et al.* (2019) studied buckling of FG nanoscale beam with porosities using nonlocal higher-order shear deformation. Khatir *et al.* (2019) proposed new technique based on Artificial Neural Network (ANN) combined with Particle Swarm Optimization (PSO) for damage quantification in laminated composite plates using Cornwell indicator (CI). Hamed *et al*. (2019) presented effects of porosity models on static behavior of size dependent functionally graded beam. Phung-Van *et al.* (2019) and Thanh *et al*. (2019b) studied porosity effects on nonlinear transient responses and stability of FG nanoplates using isogeometric analysis. Thanh *et al.* (2019c, d) studied mechanical behaviors of composite laminate microplate based on new modified couple stress theory and isogeometric analysis. Mohamed *et al.* (2019, 2020) studied postbuckling of nanotube modeled as thin beam by using energy equivalent method. Eltaher and Mohamed (2020a) developed an analytical solution to study nonlinear stability and vibration of imperfect CNTs by doublet mechanics.

Material distribution greatly affects the mechanical behavior of functionally graded structures, Alimirzaei *et al.* (2019) developed a nonlinear finite element analysis to investigate the coupled bending, buckling, and vibration behaviors of micro composite beams. Karami *et al*. (2019) investigated the buckling behavior of functionally graded (FG) nanoplate. Stability and frequency analysis of curved cantilevered microtubule were exactly investigated by Shariati *et al*. (2020). Rayleigh-Ritz's method was applied by Hussain *et al.* (2020) to simulate vibration of single-walled carbon nanotube. Using nonlocal two variables integral refined plate theory, the free vibration response of FG nanoscale plate was investigated by Balubaid *et al.* (2019). Effects of nonlocality on the vibration of different configurations of carbon nanotubes was investigated by Hussain *et al.* (2019). Based on simple nonlocal quasi 3Dhigher shear deformation theory, Boutaleb *et al.* (2019) studied the dynamic analysis of nanosized FG plates. Berghouti *et al*. (2019) studied the vibration behavior of porus FG nanoplates. Karami *et al*. (2019) analyzed the prestressed FG anisotropic nanoshell. Vibrations of FG microbeams with different material distributions was investigated by Tlidji *et al*. (2019). Thermal buckling behavior of zigzag single-walled boron nitride (SWBNNT) embedded in an elastic medium modeled as Winkler type foundation were investigated using a nonlocal first order shear deformation theory, Semmah *et al*. (2019). Bedia *et al.* (2019) analyzed both bending and buckling analysis of a nonlocal strain gradient nanobeams. Constitutive boundary conditions and paradoxes in nonlocal elastic nanobeams were adressed by Romano *et al.* (2017). This work was extended to discuss these constitutive boundary conditions for for nonlocal strain gradient elastic nano-beams, Barretta, and de Sciarra (2018). Barrett *et al.* (2019) developed a stress-driven local-nonlocal mixture model for Timoshenko nano-beams.

For perforated nanobeams, Luschi and Pieri (2014, 2016) developed closed expressions for the equivalent bending and shear stiffness of clamped–clamped beams with regular square perforations and determined their resonance frequencies. Bourouina *et al.* (2016) investigation of thermal loads and small-scale effects on free dynamics vibration of slender simply supported nonlocal perforated nanobeams with periodic square holes network. Eltaher *et al.* (2018a, b) presented a modified comprehensive model to investigate static bending, buckling and resonance frequencies of nonlocal perforated nanobeam. Kerid *et al*. (2019) explored the magnetic field, thermal loads and small-scale effects on the dynamic vibration of Euler–Bernoulli nanobeam structure composed of a rectangular configuration perforated with periodic square holes network and subjected to axial magnetic field. Eltaher and Mohamed (2020b) and Hamed *et al.* (2020) investigated mechanical behaviors of nonlocal perforated Euler-Bernoulli and Timoshenko nanobeams under general boundary conditions. Eltaher *et al*. (2020a, b) studied bending and vibration of piezoelectric nonlocal preforated nanobeam with and without surface effects by using finite element method. Almitani *et al.* (2020) investigated buckling stability of perforated nanobeams incorporating surface energy effects.

According to author’s knowledge and literature review, the investigation of the nonclassical bending behavior of perforated nanobeam with the presence of surface energy effect has not been analyzed before. So, this manuscript tends to fill this gap and present a unified nonclassical continuum model for bending analysis of regularly squared perforated nanobeams including the surface stress effects. To investigate the shear deformation effect due to perforation process, both Euler Bernoulli and Timoshenko beams theories are considered. The nonclassical theory of elasticity is coupled with the classical elasticity theory to incorporate the surface stress effects. The Gurtin-Murdoch surface elasticity model is modified and applied to simulate the surface energy effects in perforated nanobeams. Equivalent geometrical model for both bulk and surface parameters is developed. Considering both classical and nonclassical boundary conditions, closed forms for the nonclassical bending profiles throughout beam span are derived for both concentrated and uniformly distributed loading patterns. The rest of this article is organized as follows: section 2 presents equivalent geometrical and material properties of beams perforated by regularly squared array. Displacement field, strain-displacement relations, surface elasticity constitutive equations, and equilibrium equations of thin and thick perforated nanobeam are presented and derived in detail through section 3. The analytical solution procedure and the closed for expressions for different perforated nanobeams are derived in section 4. Model verification with the available analytical solutions is proved in section 5. Numerical results and comprehensive discussion are presented in section 6, to present influences of filling ratio, the number of hole rows, surface material characteristics, beam slenderness ratio as well as the boundary conditions. Section 7 discusses and illustrates main points and outcomes.

2. Equivalent geometrical model

Consider a regularly squared perforated nanobeam, shown in Fig. 1. The nanobeam has the following geometrical characteristics: length L, thickness h, and width w. The regular squared perforation pattern has the following characteristics: the spatial perforation period l_s, hole side l_s - t_s, and the number of holes throughout the cross section is N. The perforated beam filling ratio; α defined by the ratio of the spatial period, t_s to the spatial perforation period, l_s which can be expressed as

$$\alpha=\frac{t_s}{l_s},\qquad 0\le\alpha\le 1,\qquad \alpha=\begin{cases}0 & \text{Artifitial case}\\ 1 & \text{Fully filled solid beam}\end{cases} \tag{1}$$

Assume that the total induced stress throughout the cross section is the same for both fully filled solid nanobeam and the corresponding perforated one. Also, the stress distribution throughout the filled segment in the perforated nanobeam is assumed to be linear and continuous. Based on these assumptions, following the procedure presented in Luschi and Pieri (2014) and Abdelrahmaan *et al.* (2019), the equivalent bending stiffness and shear stiffness of the bulk material of the perforated nanobeam can be expressed as

$$(EI)_{Perf}=(EI)_{Solid}\left\{\frac{\alpha(N+1)(N^2+2N+\alpha^2)}{(1-\alpha^2+\alpha^3)N^3+3\alpha N^2+(3+2\alpha-3\alpha^2+\alpha^3)\alpha^2N+\alpha^3}\right\} \tag{2}$$

$$(GA)_{perf}=(EA)_{solid}\left[\frac{\alpha^3(N+1)}{2N}\right] \tag{3}$$

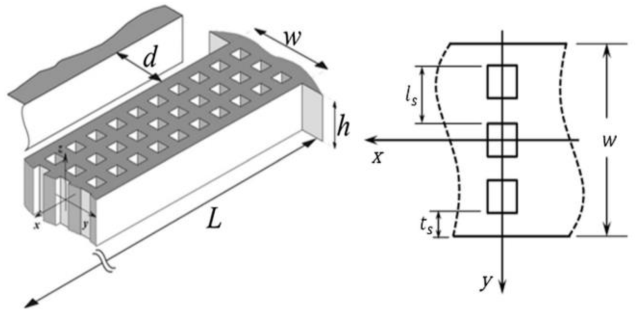

Fig. 1 Geometry of a perforated beam Luschi and Pieri (2014)

where, E is the elasticity modulus, I is the area moment of the fully filled beam. $(EA)_{solid}$ is axial extension stiffness of the full beam. The equivalent cross-sectional area of perforated nanobeam can be expressed as

$$(A)_{Perf}=\frac{(\rho A)_{solid}}{(\rho)_{Perf}}\left\{\frac{[1-N(\alpha-2)]\alpha}{N+\alpha}\right\}=(A)_{solid}\left\{\frac{[1-N(\alpha-2)]}{(N+\alpha)(2-\alpha)}\right\} \tag{4}$$

where $(A)_{Perf}$ is the equivalent cross-sectional area of the perforated beam, $(A)_{solid}$ is cross sectional area of the fully filled solid beam. Consequently, the equivalent geometrical characteristics of the surface layer can be expressed as

$$(A\tau_s)_{perf}=(A\tau_s)_{solid}\left\{\frac{[1-N(\alpha-2)]}{(N+\alpha)(2-\alpha)}\right\} \tag{5}$$

where τ_s is the surface residual stress. Then the equivalent 2nd moment of area of the perforated beam can be expressed as

$$(I)_{perf}=(I)_{solid}*\left\{\frac{[(2-\alpha)N^3+3N^2-2(\alpha-3)(\alpha^2-\alpha+1)N+\alpha^2+1]}{\{[(2-\alpha)]\}(N+\alpha)^3}\right\} \tag{6}$$

where $(I)_{perf}$ is the equivalent 2nd moment of area of the perforated beam, $(I)_{solid}$ is the 2nd moment of area of the fully filled solid beam.

3. Mathematical formulation

The mechanical behavior of beams can be modeled with different theories depending on the beam slenderness ratio. In this section, the mathematical formulation of perforated nanobeams considering surface energy effects is presented. Both Euler Bernoulli beam theory (EBBT) and Timoshenko beam theory, (TBT) are considered throughout this study.

3.1 Displacement field

Consider a straight uniform beam with the following geometrical parameters; the beam length, L and the rectangular cross-section, A and depth, h. Assuming that the deformation of the beam takes place in the *x*-*z* plane, the displacement field can be expressed in a general form as

$$\begin{aligned}u_x(x,z,t)&=u_o(x,t)-z\frac{\partial w(x,t)}{\partial x}+\gamma(z)\left(\frac{\partial w(x,t)}{\partial x}+\Phi(x,t)\right)\\ u_z(x,z,t)&=w(x,t)\end{aligned} \tag{7}$$

where (u_x, u_z) are the total displacements along the coordinate directions (x, z), and u_o, w, and Φ denote the axial, transverse and angular displacements of a point on the neutral axis. While $\gamma(z)$ is the beam shape function which can be written as, Ansari and Sahmani (2011)

$$\gamma(z)=\begin{cases}0 & EBBT\\ z & TBT\end{cases} \tag{8}$$

3.2 Strain-displacement relation

Using the linear strain-displacement relations, the components of the infinitesimal normal strain ε_{xx}, shear strain, ε_{xz} are related to the displacement and rotation vectors as, Ansari and Sahmani (2011), Yang *et al*. (2002)

$$\varepsilon_{xx}(x,t)=\begin{cases}\dfrac{\partial u_x}{\partial x}=\dfrac{\partial u_o(x,t)}{\partial x}-z\dfrac{\partial^2 w(x,t)}{\partial^2 x} & (EBBT)\\ \dfrac{\partial u_x}{\partial x}=\dfrac{\partial u_o(x,t)}{\partial x}+z\dfrac{\partial \Phi(x,t)}{\partial x} & (TBT)\end{cases} \tag{9}$$

$$\varepsilon_{xz}(x,t)=\begin{cases}0 & (EBBT)\\ \dfrac{1}{2}\left(\dfrac{\partial \mathrm{w}(x,t)}{\partial x}+\Phi(x,t)\right) & (TBT)\end{cases} \tag{10}$$

3.3 The constitutive relations

Considering the Poisson's effect, the constitutive equations are given by, Yang et al. (2002)

$$\sigma_{xx}=\begin{cases}\dfrac{(1-\nu)E}{(1+\nu)(1-2\nu)}\left(\dfrac{\partial u_o(x,t)}{\partial x}-z\dfrac{\partial^2 \mathrm{w}(x,t)}{\partial x^2}\right) & (EBBT)\\ \dfrac{(1-\nu)E}{(1+\nu)(1-2\nu)}\left(\dfrac{\partial u_o(x,t)}{\partial x}+z\dfrac{\partial \Phi(x,t)}{\partial x}\right) & (TBT)\end{cases} \tag{11}$$

$$\sigma_{yy}=\sigma_{zz}=\begin{cases}\lambda\left(\dfrac{\partial u_o(x,t)}{\partial x}-z\dfrac{\partial^2 \mathrm{w}(x,t)}{\partial x^2}\right)=\left(\dfrac{\nu}{1-\nu}\right)\sigma_{xx} & (EBBT)\\ \lambda\left(\dfrac{\partial u_o(x,t)}{\partial x}+z\dfrac{\partial \Phi(x,t)}{\partial x}\right)=\left(\dfrac{\nu}{1-\nu}\right)\sigma_{xx} & (TBT)\end{cases} \tag{12}$$

$$\sigma_{xz}=\begin{cases}2\mu\varepsilon_{xz}=0 & (EBBT)\\ 2\kappa\mu\varepsilon_{xz}=\dfrac{\kappa E}{2(1+\nu)}\left(\dfrac{\partial \mathrm{w}(x,t)}{\partial x}+\Phi(x,t)\right) & (TBT)\end{cases} \tag{13}$$

with $\hat{E}=2\mu+\lambda$ is the equivalent modulus of elasticity. Where E is the modulus of elasticity, ν is the Poison's ratio, k is the shear correction factor, σ_{xx} and σ_{xz} denote to the components of the Cauchy normal and shear stress components, respectively, λ and μ are Lame's constants in classical elasticity which are related to the elasticity modulus and Poisson's ratio as

$$\mu=\frac{E}{2(1+\nu)},\qquad \lambda=\frac{\nu E}{(1+\nu)(1-2\nu)} \tag{14}$$

3.4 The surface elasticity theory

According to the surface elasticity theory, Gurtin and Murdoch (1975, 1978), the surface layer of an elastic material satisfies distinct constitutive equations involving surface elastic constants and surface residual stress. The non-zero components of the surface stresses are related to the displacement as follows, Gurtin and Murdoch (1975, 1978)

$$\tau_{xx}=\begin{cases}\tau_s+(2\mu_s+\lambda_s)\left(\dfrac{\partial u_o(x,t)}{\partial x}-z\dfrac{\partial^2 \mathrm{w}(x,t)}{\partial x^2}\right) & (EBBT)\\ \tau_s+(2\mu_s+\lambda_s)\left(\dfrac{\partial u_o(x,t)}{\partial x}+z\dfrac{\partial \Phi(x,t)}{\partial x}\right) & (TBT)\end{cases} \tag{15}$$

$$\tau_{zx}=\tau_s n_z\ \frac{\partial \mathrm{w}(x,t)}{\partial x}\qquad (EBBT\ and\ TBT) \tag{16}$$

where n_z is the z-component of the unit outward normal vector to the beam lateral surface. μ_s and λ_s are the surface elastic constants and τ_s is the residual surface stress (i.e., the surface stress at zero strain). These three constants μ_s, λ_s and τ_s can be determined from atomistic simulations, Miller and Shenoy (2000). τ_{zx} is the out-of-plane components of the surface stress tensor. Since the stress component σ_{zz} is small as compared to σ_{xx} it is neglected in the classical beam theories. By such assumption, the surface conditions cannot be satisfied. Thus, in order to satisfy the surface conditions of the Gurtin Murdoch model, it is assumed that σ_{zz} varies linearly through the thickness of nanobeam and satisfies the balance conditions on the surfaces Wang and Feng (2007) and Lu *et al.* (2018). Therefore, σ_{zz} is given for both EBBT and TBT as follows

$$\sigma_{zz}=\frac{1}{2}\left(\sigma_{xz}^{s+}-\sigma_{xz}^{s-}\right)+\frac{z}{h}\left(\sigma_{xz}^{s+}+\sigma_{xz}^{s-}\right) \tag{17}$$

σ_{xz}^{s+} and σ_{xz}^{s-} are the top and bottom fibers' stresses, respectively. By substituting Eqs. (12) and (13), σ_{zz} can be obtained as

$$\sigma_{zz}=\frac{1}{2}\left(\tau_{nx,x}^{+}+\tau_{nx,x}^{-}\right)+\frac{z}{h}\left(\tau_{nx,x}^{+}-\tau_{nx,x}^{-}\right) \tag{18}$$

$$\sigma_{zz}=\frac{1}{2}\left(\tau_s w_{z,xx}^{+}-\tau_s w_{z,xx}^{-}\right)+\frac{z}{h}\left(\tau_s w_{z,xx}^{+}+\tau_s w_{z,xx}^{-}\right) \tag{19}$$

Eq. (19) can be rewritten as

$$\sigma_{zz}=\frac{2z}{h}\left(\tau_s\frac{\partial^2 w(x,t)}{\partial x^2}\right) \tag{20}$$

By using the expression for σ_{zz}, the components of stress for the bulk of nanobeam can be modified a

$$\sigma_{xx}=\hat{E}\varepsilon_{xx}+\nu\sigma_{zz}=\begin{cases}\hat{E}\left(\dfrac{\partial u_o(x,t)}{\partial x}-z\dfrac{\partial^2 w(x,t)}{\partial x^2}\right)+\dfrac{2\nu z}{h}\left(\tau_s\dfrac{\partial^2 w(x,t)}{\partial x^2}\right) & (EBBT)\\ \hat{E}\left(\dfrac{\partial u_o(x,t)}{\partial x}+z\dfrac{\partial \Phi(x,t)}{\partial x}\right)+\dfrac{2\nu z}{h}\left(\tau_s\dfrac{\partial^2 w(x,t)}{\partial x^2}\right) & (TBT)\end{cases} \tag{21}$$

3.5 Perforated beam equilibrium equations

According to EBBT the equilibrium equations of perforated nanobeams with surface energy effects can be written as

$$\left[\left(\hat{E}I\right)_{eq}-\frac{2\nu h}{12}(A\tau_s)_{eq}+\left(E_sI_p\right)_{eq}\right]\frac{d^4w}{dx^4}-\left[\frac{2(A\tau_s)_{eq}}{h}-P_o\right]\frac{d^2w}{dx^2}+q\ =0 \tag{22a}$$

As illustrated in Eq. (22(a)), the surface effects on the perforated Euler Bernoulli nanobeams is attributed to two terms; the surface elasticity (E_s) and surface residual stresses (surface tension), τ_s. Neglecting the surface residual stress effect, the equilibrium equation can be expressed as

$$\left[\left(\hat{E}I\right)_{eq}+\left(E_sI_p\right)_{eq}\right]\frac{d^4w}{dx^4}+P_o\frac{d^2w}{dx^2}+q\ =0 \tag{22b}$$

While if the surface elasticity effect is neglected, the equilibrium equation can be expressed for perforated Euler Bernoulli nanobeam PEBNB with surface tension only can be written as

$$\left[\left(\hat{E}I\right)_{eq}-\frac{2\nu h}{12}(A\tau_s)_{eq}\right]\frac{d^4w}{dx^4}-\left[\frac{2(A\tau_s)_{eq}}{h}-P_o\right]\frac{d^2w}{dx^2}+q=0 \tag{22c}$$

Neglecting the surface elasticity effects leads to the classical EBB equilibrium equation which can be written as

$$\left[\left(\hat{E}I\right)_{eq}\right]\frac{d^4w}{dx^4}+P_o\frac{d^2w}{dx^2}+q\ =0 \tag{22d}$$

Considering the TBT, the equilibrium equations can be expressed as

$$\frac{2\nu}{h}(I\tau_s)_{eq}\frac{d^3w}{dx^3}+\left[\left(\hat{E}I\right)_{eq}+\left(E_sI_p\right)_{eq}\right]\frac{d^2\Phi}{dx^2}-\kappa(GA)_{eq}\left(\Phi+\frac{dw}{dx}\right)=0 \tag{23a}$$

$$\left(\frac{2}{h}(A\tau_s)_{eq}+\kappa(GA)_{eq}-P_0\right)\frac{d^2w}{dx^2}+\kappa(GA)_{eq}\frac{d\Phi}{dx}+q=0 \tag{24a}$$

Neglecting the surface elasticity effect, the equilibrium equations of perforated Timoshenko nanobeam (PTNB) with the presence of surface residual stress only can be written as.

$$\frac{2\nu}{h}(I\tau_s)_{eq}\frac{d^3w}{dx^3}+\left[\left(\hat{E}I\right)_{eq}\right]\frac{d^2\Phi}{dx^2}-\kappa(GA)_{eq}\left(\Phi+\frac{dw}{dx}\right)=0 \tag{23b}$$

$$\left(\frac{2}{h}(A\tau_s)_{eq}+\kappa(GA)_{eq}-P_0\right)\frac{d^2w}{dx^2}+\kappa(GA)_{eq}\frac{d\Phi}{dx}+q=0 \tag{24b}$$

On the other hand neglecting the surface residual stress and considering the surface elasticity effect only leads to the following equilibrium equations

$$\left[\left(\hat{E}I\right)_{eq}+\left(E_sI_p\right)_{eq}\right]\frac{d^2\Phi}{dx^2}-\kappa(GA)_{eq}\left(\Phi+\frac{dw}{dx}\right)=0 \tag{23c}$$

$$\left(\kappa(GA)_{eq}-P_0\right)\frac{d^2w}{dx^2}+\kappa(GA)_{eq}\frac{d\Phi}{dx}+q=0 \tag{24c}$$

Neglecting the two effects of the surface elasticity lead to the well known classical TBT with the following equilibrium equations

$$\left[\left(\hat{E}I\right)_{eq}+\left(E_sI_p\right)_{eq}\right]\frac{d^2\Phi}{dx^2}-\kappa(GA)_{eq}\left(\Phi+\frac{dw}{dx}\right)=0 \tag{23d}$$

$$\left(\kappa(GA)_{eq}-P_0\right)\frac{d^2w}{dx^2}+\kappa(GA)_{eq}\frac{d\Phi}{dx}+q=0 \tag{24d}$$

Assuming rectangular cross-sectional area of the perforated nanobeam

$$\left(E_sI_p\right)_{eq}=E_s\left(\frac{(A)_{eq}h}{2}+\frac{h^3}{6}\right)\ and \qquad (I\tau_s)_{eq}=\frac{h^2}{12}\ (A\tau_s)_{eq} \tag{25}$$

4. Analytical solution

In this section, closed form solutions for static deflection profile throughout the perforated nanobeam with different nonclassical boundary conditions considering both PEBBT and PTBT theories are presented. Introducing the nondimensional quantities; $\bar{w}=\frac{w}{L}$ and $\bar{x}=\frac{x}{L}$. additionally, $\bar{M},\bar{\Phi}$ and $\bar{Q}$ are defined in terms of the nondimensional quantities $\bar{w}$ and $\bar{x}$ the quantities. The considered boundary conditions shown in Table (1).

4.1 Perforated Euler Bernoulli nanobeams (PEBNBs)

To obtain closed form solution for static deflection of PEBNBs, the following non-dimensional quantities are defined

$$\bar{w}=\frac{w}{L}, \qquad \bar{x}=\frac{x}{L} \qquad \text{and} \qquad \frac{\partial w}{\partial x}=\frac{\partial\bar{w}}{\partial\bar{x}} \tag{26}$$

The governing equation of PEBNBs subjected to uniformly distributed load of intensity q, the bending moment (M^E) and the shear force (Q^E), in terms of the non-dimensional quantities, $\bar{w}$ and $\bar{x}$ can be written as

Table 1 The different boundary conditions for both distributed and central point loads

BCs	Distributed load
S-S	$\bar{w}(0)=\bar{w}(1)=\bar{M}(0)=\bar{M}(1)=0$
C-C	$\bar{w}(0)=\bar{\Phi}(0)=\bar{w}(1)=\bar{\Phi}(1)=0$
C-F	$\bar{w}(0)=\bar{\Phi}(0)=\bar{M}(1)=\bar{Q}(1)=0$
BCs	Point load of intensity P
S-S	$\bar{w}(0)=\bar{M}(0)=\bar{\Phi}(1/2)=0,\quad \bar{Q}(1/2)=\frac{-P}{2}$
C-C	$\bar{w}(0)=\bar{\Phi}(0)=\bar{\Phi}(1/2)=0,\quad \bar{Q}(1/2)=\frac{-P}{2}$
C-F	$\bar{w}(0)=\bar{\Phi}(0)=0,\quad \bar{M}(1)=0,\quad \bar{Q}(l)=-P$

$$\frac{d^4\bar{w}}{d\bar{x}^4}-\beta_E^2\frac{d^2\bar{w}}{d\bar{x}^2}=-\frac{q\ L^3}{K_b^E} \tag{27a}$$

$$M^E=-\frac{K_b^E}{L}\frac{\partial^2\bar{w}}{\partial\bar{x}^2},\qquad Q^E=-\frac{K_b^E}{L^2}\frac{\partial^3\bar{w}}{\partial\bar{x}^3}+\frac{2(A)_{eq}}{h}\tau_s\frac{\partial\bar{w}}{\partial\bar{x}} \tag{27b}$$

Where

$$K_b^E=\left[\left(\hat{E}I\right)_{eq}-\frac{2\nu h}{12}(A\tau_s)_{eq}+E_s\left(\frac{(A)_{eq}h}{2}+\frac{h^3}{6}\right)\right]$$

$$\beta_E^2=\frac{\frac{2(A)_{eq}}{h}\tau_s\times L^2}{K_b^E}$$

The general solution of Eq. (27(a)) for both the static deflection and rotation can be written as

$$\bar{w}(\bar{x})=C_1\exp(\beta_E\bar{x})+C_2\exp(-\beta_E\bar{x})+\frac{qL^3}{2\beta_E^2K_b^E}\bar{x}^2+C_3\bar{x}+C_4 \tag{28a}$$

$$\bar{\Phi}(\bar{x})=\bar{w}'(\bar{x})=C_1L\beta_E\exp(\beta_E\bar{x})-L\beta_EC_2\exp(-\beta_E\bar{x})+\frac{qL^4}{\beta_E^2K_b^E}\bar{x}+\ C_3L \tag{28b}$$

The bending moment and the shear force can be written as

$$M^E(\bar{x})=-\frac{K_b^E}{L}\left(C_1\beta_E^2\exp(\beta_E\bar{x})+C_2\beta_E^2\exp(-\beta_E\bar{x})+\frac{qL^3}{\beta_E^2K_b^E}\right) \tag{29a}$$

$$Q^E(\bar{x})=-\frac{K_b^E}{L^2}\left(C_1\beta_E^3\exp(\beta_E\bar{x})-C_2\beta_E^3\exp(-\beta_E\bar{x})\right)+\frac{2(A)_{eq}}{h}\tau_s\left(C_1\beta_E\exp(\beta_E\bar{x})-C_2\beta_E\exp(-\beta_E\bar{x})+\frac{qL^3}{\beta_E K_b^E}\bar{x}+C_3\right) \tag{29b}$$

Apply the different boundary conditions shown in Table 1. The following explicit formulas can be obtained for the static deflection profile throughout the beam span

4.1.1 Simply Supported (S -S) beams

For the simply supported beam (*S-S*) under uniform distributed load of intensity q, the nonclassical static bending deflection, $[\bar{w}(\bar{x})]_{NCL}$ can be expressed as

$$[\bar{w}(\bar{x})]_{NCL} = -\frac{qL^3}{\beta_E^4 K_b^E}\left(\frac{\exp(\beta_E \bar{x})}{1+\exp(\beta_E)} + \frac{\exp(\beta_E)\exp(-\beta_E \bar{x})}{1+\exp(\beta_E)} - \frac{\beta_E^2}{2}\bar{x}^2 + \frac{\beta_E^2}{2}\bar{x} - 1\right) \quad (30a)$$

Neglecting the surface energy effects, the classical bending deflection $[\bar{w}(\bar{x})]_{CL}$ can be written as

$$[\bar{w}(\bar{x})]_{CL} = \frac{qL^3 \bar{x}}{24K_b^E}[-\bar{x}^3 + 2\bar{x}^2 - 1\ ] \quad (30b)$$

By the same way, the nonclassical static bending deflection for S-S beam under central point load of intensity p, $[\bar{w}(\bar{x})]_{NCL}$ can be expressed as

$$[\bar{w}(\bar{x})]_{NCL} = \frac{PL^2}{2\beta_E^2 \times K_b^E}\left[\frac{\exp(0.5\beta_E)\times\exp(\beta_E \bar{x})}{\beta_E(1+\exp(\beta_E))} - \frac{\exp(0.5\beta_E)\times\exp(-\beta_E \bar{x})}{\beta_E(1+\exp(\beta_E))} - \bar{x}\right] \quad (31a)$$

The classical solution can be obtained when the surface energy effects are neglected and can be expressed as

$$[\bar{w}(\bar{x})]_{CL} = \frac{PL^2 \bar{x}}{48K_b^E}(4\bar{x}^2\ \ - 3) \quad (31b)$$

4.1.2 Clamped-Clamped (C-C) beams

Considering the clamped-clamped beam under uniform distributed load of intensity q, the nonclassical bending deflection can be obtained as

$$[\bar{w}(\bar{x})]_{NCL} = \frac{-qL^3}{2\beta_E^2 \times K_b^E}\left[\frac{\exp(\beta_E \bar{x})}{\beta_E\ (\exp(\beta_E)-1)} + \frac{\exp(\beta_E)\times\exp(-\beta_E \bar{x})}{\beta_E(\exp(\beta_E)-1)} - \bar{x}^2 + \bar{x} - \frac{(\exp(\beta_E)+1)}{\beta_E\ (\exp(\beta_E)-1)}\right] \quad (32a)$$

While the classical bending deflection can be obtained as

$$[\bar{w}(\bar{x})]_{CL} = \frac{-q\bar{x}^2 L^3}{24K_b^E}(1 - \bar{x}\ \ )^2 \quad (32b)$$

By the same way, the nonclassical static bending deflection for C-C beam under central point load can be obtained as

$$[\bar{w}(\bar{x})]_{NCL} = \frac{PL^2}{2\beta_E^2 \times K_b^E}\left[\frac{\exp(\beta_E \bar{x})}{\beta_E\ (1+\exp(0.5\beta_E))} - \frac{\exp(0.5\beta_E)\times\exp(-\beta_E \bar{x})}{\beta_E(1+\exp(0.5\beta_E))} - \bar{x} + \frac{(exp(0.5\beta_E)-1)}{\beta_E(1+\exp(0.5\beta_E))}\right] \quad (33a)$$

The classical bending deflection can be expressed as

$$[\bar{w}(\bar{x})]_{CL} = \frac{PL^2 \bar{x}^2}{48K_b^E}(4\bar{x}\ \ - 3) \quad (33b)$$

4.1.3 Clamped- Free(C-F) beams

The nonclassical bending deflection of cantilever beam (C-F) under uniformly distributed load can be expressed as

$$[\bar{w}(\bar{x})]_{NCL} = \frac{-qL^3}{\beta_E^2 \times K_b^E}\left[\frac{(1-\beta_E\exp(-\beta_E))\exp(\beta_E \bar{x})}{\beta_E^2\ (\exp(\beta_E)+\exp(-\beta_E))} + \frac{(1+\beta_E\exp(\beta_E))\exp(-\beta_E \bar{x})}{\beta_E^2\ (\exp(\beta_E)+\exp(-\beta_E))} - \frac{\bar{x}^2}{2} + \bar{x} - \frac{(2-\beta_E\exp(-\beta_E)+\beta_E\exp(\beta_E))}{\beta_E^2\ (\exp(\beta_E)+\exp(-\beta_E))}\right] \quad (34a)$$

The classical bending deflection can be expressed as

$$[\bar{w}(\bar{x})]_{CL} = \frac{q\bar{x}^2 L^3}{24K_b^E}(-\bar{x}^2 + 4\bar{x} - 6) \quad (34b)$$

By the same way, the nonclassical static bending deflection of cantilever beam under tip point load can be obtained as

$$[\bar{w}(\bar{x})]_{NCL} = \frac{PL^2}{\beta_E^2 \times K_b^E}\left[\frac{\exp(\beta_E \bar{x})}{\beta_E\ (\exp(2\beta_E)+1)} - \frac{\exp(2\beta_E)\exp(-\beta_E \bar{x})}{\beta_E\ (\exp(2\beta_E)+1)} - \bar{x} + \frac{(exp(2\beta_E)-1)}{\beta_E\ (\exp(2\beta_E)+1)}\right] \quad (35a)$$

Neglecting the surface energy effects, the classical bending deflection can be obtained as

$$[\bar{w}(\bar{x})]_{CL} = \frac{P\bar{x}^2 L^2}{6K_b^E}(\bar{x}\ \ - 3) \quad (35b)$$

4.2 Perforated Timoshenko nanobeams (PTNBs)

The equilibrium equations of PTNBs subjected to uniformly distributed load of intensity q, the bending moment (M^T) and the shear force (Q^T) can be written a

$$\frac{2\nu}{h}(I\tau_s)_{eq}\frac{d^3 w}{dx^3} + \left[\left(\hat{E}I\right)_{eq} + \left(E_s I_p\right)_{eq}\right]\frac{d^2\Phi}{dx^2} - \kappa(GA)_{eq}\left(\Phi + \frac{dw}{dx}\right)\ \ = 0 \quad (36a)$$

$$\left(\frac{2}{h}(A\tau_s)_{eq} + \kappa(GA)_{eq} - N_0\right)\frac{d^2 w}{dx^2} + \kappa(GA)_{eq}\frac{d\Phi}{dx} + q = 0 \quad (36b)$$

The bending moment can be expressed as

$$M^T = \int_A \sigma_{xx} z dA + \oint_S \tau_{xx} z ds = \left((E_s I_s)_{eq} + \left(\hat{E}I\right)_{eq}\right)\frac{\partial\Phi(x,t)}{\partial x} + \left(\frac{2\nu(I\tau_s)_{eq}}{h}\right)\frac{\partial^2 w_o(x,t)}{\partial x^2} + \tau_s P_A \quad (36c)$$

where

$$I = \int_A z^2 dA, \qquad I_s = \oint_S z^2 ds\ , \qquad P_A = \oint_S z ds \qquad S_P = \oint_S n_z^2 ds \quad (36d)$$

The shear force can be expressed as

$$Q^T = \int_A \sigma_{xz} dA + \oint_S \tau_{xz} n_z^2 ds = \kappa(GA)_{eq}\left(\frac{\partial \mathrm{w}(x,t)}{\partial x} + \Phi(x,t)\right) + \left(S_p \tau_s\right)_{eq}\frac{\partial w_o(x,t)}{\partial x} \quad (36e)$$

Using Eqs. (39(a)) and (39(b)), the PTNBs equilibrium equation can be expressed in a single equation in terms of the transverse deflection. Neglect the effect of the compressive force, N_0, integrating Eq. (39(b)), the rotation, Φ can be obtained as

$$\Phi = -\frac{1}{\kappa(GA)_{eq}}\left[\left(\frac{2}{h}(A\tau_s)_{eq} + \kappa(GA)_{eq}\right)\frac{d\bar{w}}{d\bar{x}} - q\bar{x}L + C_3\ \right] \quad (36f)$$

The 1st and the 2nd derivatives of the rotation can be expressed as

$$\frac{d\Phi}{dx} = -\frac{1}{\kappa(GA)_{eq}}\left[\left(\frac{2}{h}(A\tau_s)_{eq} + \kappa(GA)_{eq}\right)\frac{d^2\overline{w}}{Ld\bar{x}^2} - q\ \right] \quad (36g)$$

$$\frac{d^2\Phi}{dx^2} = -\frac{1}{\kappa(GA)_{eq}}\left[\left(\frac{2}{h}(A\tau_s)_{eq} + \kappa(GA)_{eq}\right)\frac{d^3\overline{w}}{L^2d\bar{x}^3}\ \right] \quad (36h)$$

Substitute into Eq. (39(a)) yield

$$\left[\left[(\hat{E}I)_{eq} + (E_sI_p)_{eq}\right]\left(\frac{\frac{2}{h}(A\tau_s)_{eq}}{\kappa(GA)_{eq}} + 1\right) - \frac{2\nu}{h}(I\tau_s)_{eq}\right]\frac{d^3\overline{w}}{d\bar{x}^3} - \left(\frac{2}{h}(A\tau_s)_{eq}\right)L^2\frac{d\overline{w}}{d\bar{x}} + qL^3\bar{x} - C_3L^2 \ = 0 \quad (36i)$$

Eq. (39(i)) can be written as

$$\frac{d^3\overline{w}}{d\bar{x}^3} - \beta_T^2\frac{d\overline{w}}{d\bar{x}} + \frac{qL^3}{K_s^T}\bar{x} - \frac{C_3L^2}{K_s^T} = 0 \quad (36j)$$

Integrating yields

$$\frac{d^2\overline{w}}{d\bar{x}^2} - \beta_T^2\overline{w} = -\frac{qL^3}{2K_s^T}\bar{x}^2 + \frac{C_3L^2}{K_s^T}\bar{x} + C_4 \quad (36k)$$

Where

$$K_s^T = \left\{\gamma_T \times \left[(\hat{E}I)_{eq} + (E_sI_p)_{eq}\right] - \frac{2\nu}{h}(I\tau_s)_{eq}\right\},$$
$$\beta_T^2 = \frac{L^2\frac{2}{h}(A\tau_s)_{eq}}{K_s^T} \quad (36i)$$
$$\gamma_T = \left[\frac{\frac{2}{h}(A\tau_s)_{eq}}{\kappa(GA)_{eq}} + 1\right]$$

The general solution of Eq. (39.k) can be written as

$$\overline{w}(\bar{x}) = C_1\exp(\beta_T\bar{x}) + C_2\exp(-\beta_T\bar{x}) + \frac{qL^3}{2\beta_T^2K_s^T}\bar{x}^2 - \frac{C_3L^2}{K_s^T\beta_T^2}\bar{x} + C_4 \quad (37a)$$

$$\Phi(\bar{x}) = \left[-\left(\frac{\frac{2}{h}(A\tau_s)_{eq}}{\kappa(GA)_{eq}} + 1\right)(C_1\beta_T\exp(\beta_T\bar{x}) - \beta_TC_2\exp(-\beta_T\bar{x})\ ) - \frac{qL^3\bar{x}}{\beta_T^2K_s^T} + \frac{C_3L^2}{K_s^T\beta_T^2}\right] \quad (37b)$$

The bending moment and the shear force can be written as

$$M^T(\bar{x}) = -\left[K_s^T(C_1(\beta_T)^2\exp(\beta_T\bar{x}) + (\beta_T)^2C_2\exp(-\beta_T\bar{x})\ ) + K_b\frac{qL^3}{\beta_T^2K_s^T}\right] \quad (37c)$$

$$Q^T(\bar{x}) = qL\bar{x} - C_3 \quad (37d)$$

Neglecting the surface tension ($\beta_T^2 = 0$)

$$\frac{\partial^3\overline{w}}{\partial\bar{x}^3} = -\frac{qL^3}{K_s^T}\bar{x} + \frac{C_3L^2}{K_s^T} \quad (38a)$$

where

$$K_s^T = \left[(\hat{E}I)_{eq} + (E_sI_p)_{eq}\right] \quad (38b)$$

Integrating Eq. (41(a)) yields

$$\overline{w}(\bar{x}) = -\frac{qL^3}{24K_s^T}\bar{x}^4 + \frac{C_3L^2}{6K_s^T}\bar{x}^3 + \frac{C_2}{2}\bar{x}^2 + C_1\ \bar{x} \quad (38c)$$

$$\Phi(\bar{x}) = -\ \left[-\frac{qL^3}{6K_s^T}\bar{x}^3 + C_3\left(\frac{L^2}{2K_s^T}\bar{x}^2 + \frac{1}{\kappa(GA)_{eq}}\right) + C_2\bar{x} + C_1 \quad - \frac{q\bar{x}L}{(GA)_{eq}}\right] \quad (38d)$$

The bending moment and the shear force can be written as

$$M^T(\bar{x}) = K_s^T\frac{\partial\Phi}{\partial x} = -\frac{K_s^T}{L}\left[\frac{\partial^2\overline{w}}{\partial\bar{x}^2} - \frac{qL}{\kappa(GA)_{eq}}\right] == -\frac{K_s^T}{L}\left[-\frac{qL^3}{2K_s^T}\bar{x}^2 + C_3\left(\frac{L^2}{K_s^T}\bar{x}\right) + C_2 - \frac{qL}{(GA)_{eq}}\right] \quad (38e)$$

$$Q^T = \kappa(GA)_{eq}\left(\frac{dw}{dx} + \varphi\right) = qL\bar{x} - C_3 \quad (38f)$$

Apply the different boundary conditions shown in Table 1. Explicit formulas can be obtained for the static deflection profile throughout the beam span.

4.2.1 Simply Supported (S -S) beams

For the simply supported beam (*S-S*) under uniform distributed load of intensity q, the nonclassical static bending deflection, $[\overline{w}(\bar{x})]_{NCL}^T$ can be expressed as

$$[\overline{w}(\bar{x})]_{NCL}^T = -\frac{K_bqL^3}{\beta_T^4(K_s^T)^2}\left(\left[\frac{1-\exp(-\beta_T)}{\exp(\beta_T)-\exp(-\beta_T)}\right]\exp(\beta_T\bar{x}) + \left[\frac{\exp(\beta_T)-1}{\exp(\beta_T)-\exp(-\beta_T)}\right]\exp(-\beta_T\bar{x}) - \frac{K_s^T\beta_T^2}{2\times K_b}\bar{x}^2 + \frac{K_s^T\ \beta_T^2}{2\times K_b}\bar{x} - 1\right) \quad (39a)$$

Neglecting the effect of surface energy effects, the classical bending deflection $[\overline{w}(\bar{x})]_{CL}$ can be written as

$$[\overline{w}(\bar{x})]_{CL}^T = \frac{qL^3\bar{x}}{24K_s^T}(-\bar{x}^3 + 2\bar{x}^2 - \ 1) + \frac{q\bar{x}\ L}{2\kappa(GA)_{eq}}(\bar{x}^2 - 1\ ) \quad (39b)$$

By the same way, the nonclassical static bending deflection for S-S beam under central point load of intensity p, $[\overline{w}(\bar{x})]_{NCL}$ can be expressed as

$$[\overline{w}(\bar{x})]_{NCL}^T = \frac{PL^2[\exp(\beta_T\bar{x})-\exp(-\beta_T\bar{x})]}{2K_s^T\beta_T^3\ \gamma_T(\exp(0.5\beta_T)+\exp(-0.5\beta_T)\ )} - \frac{PL^2}{2K_s^T\beta_T^2}\bar{x} \quad (40a)$$

The classical solution can be obtained when the surface energy effects are neglected and can be expressed as

$$[\overline{w}(\bar{x})]_{CL}^T = \frac{P\bar{x}L^2}{48K_b^E}(4\bar{x}^2 \ - 3) - \frac{P\bar{x}}{2\kappa(GA)_{eq}} \quad (40b)$$

4.2.2 Clamped-Clamped (C-C) beams

Considering the clamped-clamped beam under uniform distributed load of intensity q, the nonclassical bending deflection can be obtained as

$$[\overline{w}(\bar{x})]_{NCL}^T = \frac{-qL^3}{2\beta_T^3K_s^T}\left(\left[\frac{\exp(\beta_T\bar{x})+\exp(\beta_E)\exp(-\beta_T\bar{x})-(\exp(\beta_T)+1)}{\gamma_T(\exp(\beta_T)-1)}\right] - \beta_T\bar{x}(\bar{x}-1)\right) \quad (41a)$$

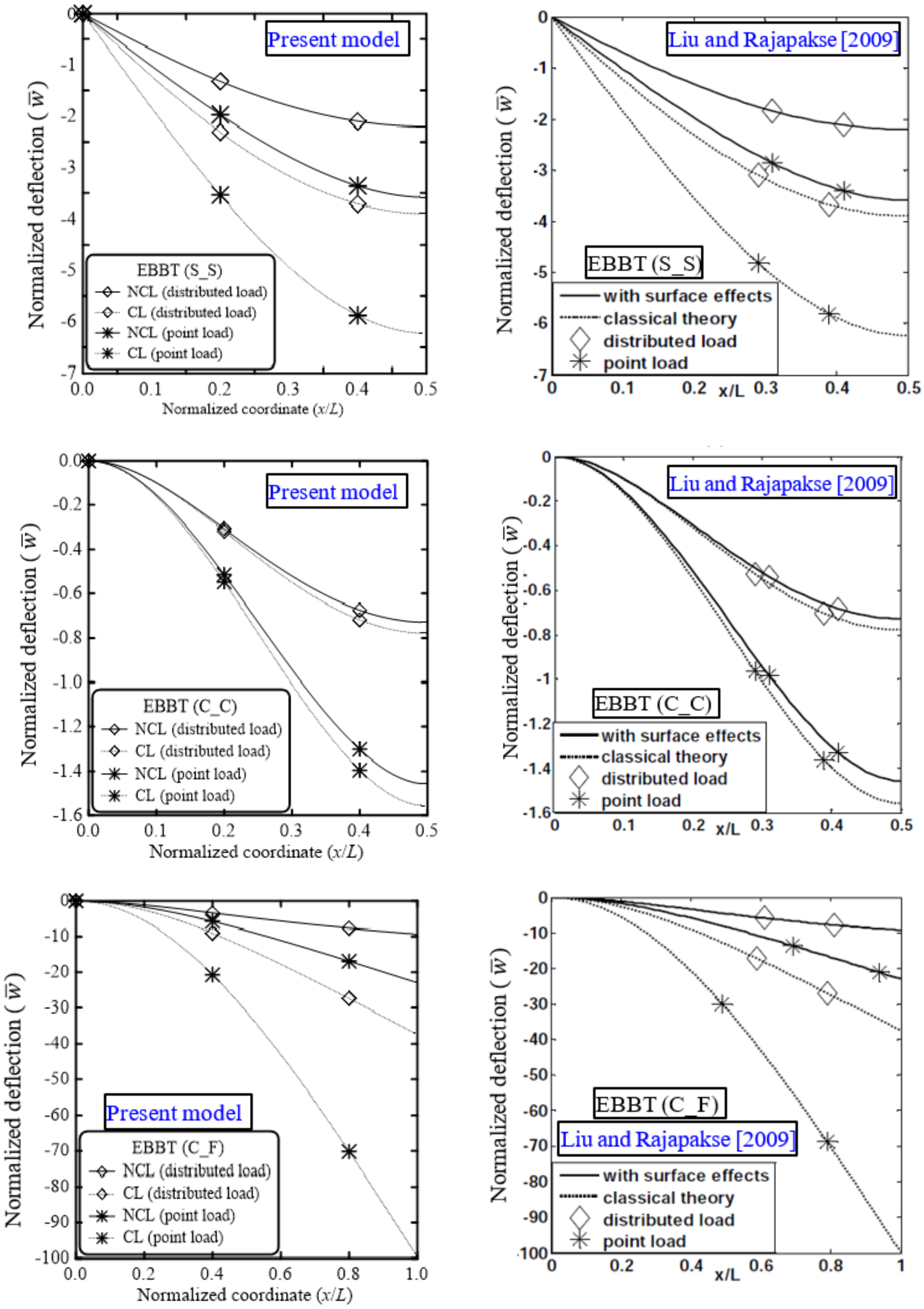

Fig. 2 Variation of the normalized deflection with the normalized coordinate for EBBT for different loading and boundary conditions

While the classical bending deflection can be obtained as

$$[\bar{w}(\bar{x})]^T_{CL} = \frac{-q\bar{x}^2L^3}{24K^T_S}(1-\bar{x}\ )^2 + \frac{qL}{2(GA)_{eq}}(\bar{x}^2-1) \quad (41b)$$

By the same way, the nonclassical static bending deflection for C-C beam under central point load can be obtained as

$$[\bar{w}(\bar{x})]^T_{NCL} = \frac{PL^2}{2K^T_S\beta^3_T\gamma_T\left(\exp\left(\frac{\beta_T}{2}\right)-\exp\left(\frac{-\beta_T}{2}\right)\right)} \left[\left(1-\exp\left(\frac{-\beta_T}{2}\right)\right)\exp(\beta_T\bar{x}) + \left(1-\exp\left(\frac{\beta_T}{2}\right)\right)\exp(-\beta_T\bar{x}) + \exp\left(\frac{\beta_T}{2}\right) + \exp\left(\frac{-\beta_T}{2}\right) - 2\right] - \frac{PL^2}{2K^T_S\beta^2_T}\bar{x} \quad (42a)$$

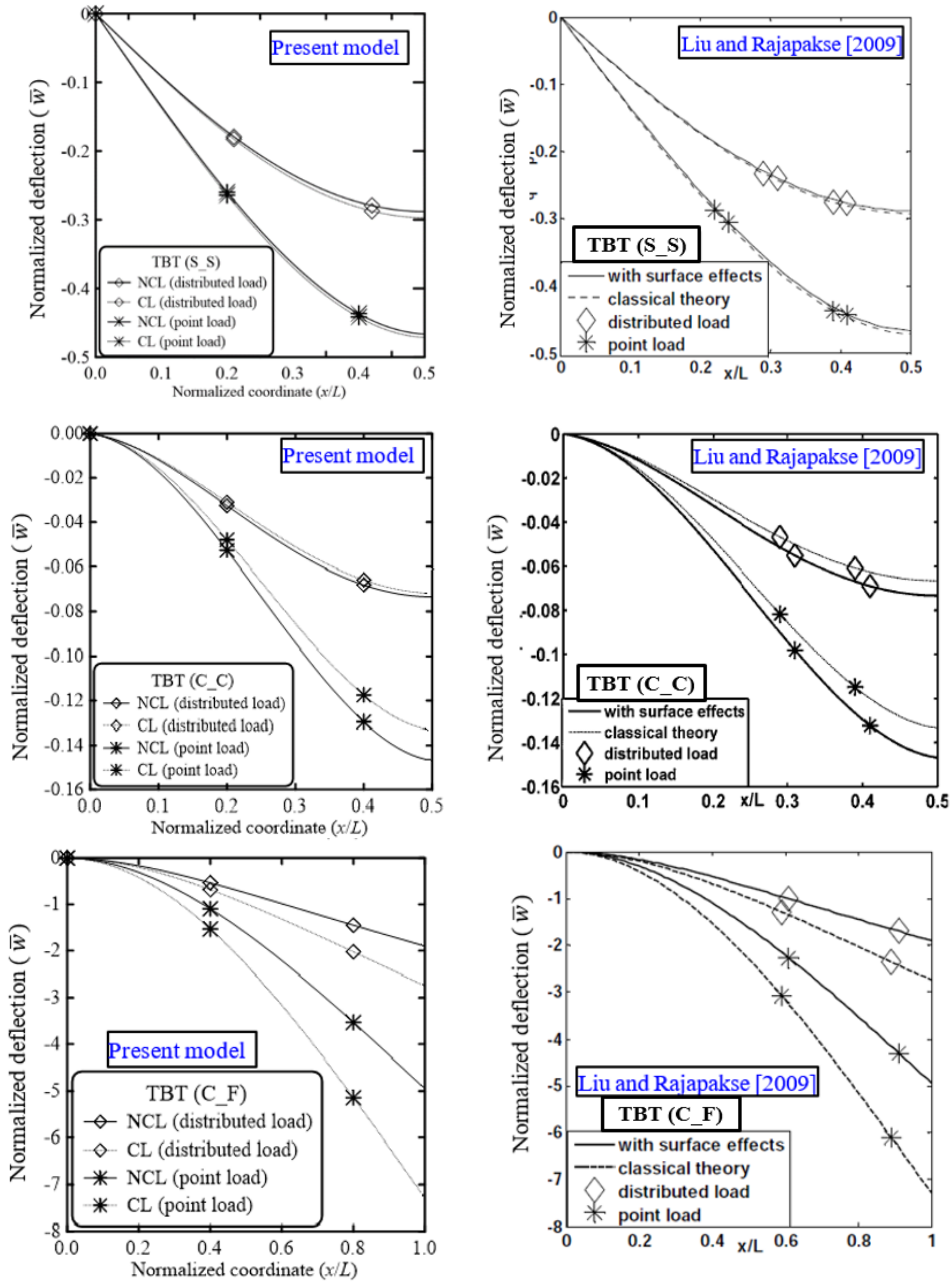

Fig. 3 Variation of the normalized deflection with the normalized coordinate for TBT for different loading and boundary conditions

The classical bending deflection can be expressed as

$$[\bar{w}(\bar{x})]^T_{CL} = \frac{P\bar{x}^2L^2}{48K_s^T}(4\bar{x} - 3) - \frac{P\ \bar{x}}{2\kappa(GA)_{eq}} \qquad (42b)$$

4.2.3 Clamped- Free(C-F) beams

The nonclassical bending deflection of cantilever beam (C-F) under uniformly distributed load can be expressed as

$$[\bar{w}(\bar{x})]^T_{NCL} = \frac{\left(\frac{qL^3}{K_s^T\beta_T^2}\right)}{(\exp(\beta_T)+\exp(-\beta_T))}\left\{\left[\frac{\exp(-\beta_T)}{\beta_T \times \gamma_T} - \frac{K_b}{\beta_T^2(K_s^T)}\right]\exp(\beta_T\bar{x}) - \left[\frac{\exp(\beta_T)}{\beta_T \times \gamma_T} + \frac{K_b}{\beta_T^2(K_s^T)}\right]\exp(-\beta_T\bar{x}) + \left[\frac{\exp(\beta_T)-\exp(-\beta_T)}{\beta_T \times \gamma_T} + \frac{2K_b}{\beta_T^2(K_s^T)}\right]\right\} + \frac{qL^3\bar{x}}{2\beta_T^2K_s^T}(\bar{x}-2) \qquad (43a)$$

While the classical bending deflection can be obtained as

$$[\bar{w}(\bar{x})]_{CL}^{T} = -\frac{q\bar{x}^2L^3}{24K_s^T}(\bar{x}^2 - 4\bar{x} + 6 \quad) + \frac{qL\bar{x}}{2\kappa(GA)_{eq}}(x-2) \quad (43b)$$

By the same way, the nonclassical static bending deflection of cantilever beam under tip point load can be obtained as

$$[\bar{w}(\bar{x})]_{NCL}^{T} = \frac{PL^2[\exp(-\beta_T)\exp(\beta_T\bar{x}) - \exp(\beta_T)\exp(-\beta_T\bar{x}) + \exp(\beta_T) - \exp(-\beta_T)]}{K_s^T\beta_T^3 \times \gamma_T(\exp(\beta_T) + \exp(-\beta_T))} - \frac{PL^2}{K_s^T\beta_T^2}\bar{x} \quad (44a)$$

Neglecting the surface energy effects, the classical bending deflection can be obtained as

$$[\bar{w}(\bar{x})]_{CL}^{T} = \frac{P\bar{x}^2L^2}{6K_s^T}(\bar{x} \quad - 3) - \frac{P\ \bar{x}}{\kappa(GA)_{eq}} \quad (44b)$$

5. Model verification

To verify the developed procedure to investigate the nonclassical deflection for nanoscale beam, consider a nanoscale beam made of aluminum silicon (Si) having the following bulk and surface properties; Liu and Rajapakse (2009): E=107 GPa, ν=0.33, and ρ=2330 kg/m^3. The surface characteristics are; τ^s= 0.6056 N/m, u_s= - 2.7779 N/m, λ_s=-4.4939 N/m. The dimensions for thin beams are L =120 nm, H = 6 nm and w = 3 nm, and those for thick beams are L = 50 nm, H = 6 nm and w = 3 nm. Based on both EBBT and TBT the problem is solved under different loading and boundary conditions for both nonclassical and classical theories. The same problem was analytically solved by Liu and Rajapakse (2009) under the same boundary and loading conditions. The obtained results are compared with that obtained by Liu and Rajapakse (2009). As depicted in Figs. 2 and 3, it is illustrated that an excellent agreement is found.

6. Numerical results

To demonstrate the salient features of the mechanical behavior of perforated nanobeams incorporating the surface energy effect for different geometry, loading and boundary conditions. Beams are made of silicon (Si); Liu and Rajapakse (2009). The dimensions for thin beams are h = 6nm, b = 3nm, L = 60 nm and ν=0.33 for both buckling and static bending analyses.

The dependency of the maximum nondimensional transverse deflection (ω_{max}=w/L) on the perforated beam filling ratio due to distributed ($W_{Q\max}$) and concentrated ($W_{P\max}$) loads for both PEBBT and PTBT for different BCs is illustrated in Fig. 4. It is noticed that both the maximum nondimensional transverse deflection is decreased with increasing the perforated beam filling ratio due to increasing the beam rigidity. Moreover, the difference between the nonclassical and classical transverse deflection is also decreased due to increasing the bulk volume compared to the perforated beam surface area. Incorporating the shear deformation effect in PTBT increases the perforated beam flexibility consequently higher values of $\omega_{\max}$ is detected compared with the corresponding PEBBT. Moreover, the applied loading pattern significantly affects the maximum nondimensional transverse deflection, higher value of $\omega_{\max}$ is detected for the concentrated load pattern compared with the corresponding distributed load pattern.

The beam aspect ratio (L/h) significantly affects the investigated values of the maximum nondimensional transverse deflection. Increasing the perforated beam aspect ratio results in higher values of $\omega_{\max}$. Also, the deviation between the classical and nonclassical values is increased due to increasing the surface are to bulk volume ratio. As shown in Fig. 5, although the perforated beam aspect ratio reaches 40 considerable deviation between the detected values of $\omega_{\max}$ for both PEBBT and PTBT is noticed for both C_C and S_S BCs especially at lower values of filling ratio while almost the same response is noticed for C_F BCs.

Variations of ω_{max} with the number of hole rows (N) beam filling ratio (α=0.5) for both thick and thin perforated beams are illustrated in Figs. (6) and (7), respectively for distributed and concentrated load patterns for different boundary conditions. It is depicted that ω_{max} increases with increasing the number of hole rows due to increasing the perforated beam flexibility. Moreover more increase in ω_{max} is detected for PTBT due to the shear deformation effect which increases the beam flexibility. Increasing the beam aspect ratio results in higher values of both ωmax and the difference between the classical and nonclassical values of ω_{max}. On the other hand, although the beam aspect ratio reaches 4, a noticeable deviation between the detected values of ω_{max} for both PTBT and PEBBT C_C BCs while almost the same response is detected for C_F and S_S BCs.

7. Conclusions

An analytical methodology capable of investigating the nonclassical bending deflection for perforated nanobeams incorporating the surface stress effects is presented. An equivalent geometrical model for both bulk and surface characteristics is developed. Based on the developed geometrical model, the Gurtin-Murdoch (GM) surface elasticity theory is adopted to incorporate the surface energy effects. Regularly squared cutout configuration is considered through perforation process. Both PEBBT and PTBT are considered to explore the shear deformation effect associated with the perforation process. Considering both classical and nonclassical boundary conditions, explicit closed forms for the nonclassical bending deflection are developed relevant to each type of beam theory considering both concentrated and uniformly distributed loading patterns. The proposed non-classical procedure is verified by comparing the obtained results with the available analytical and solution and an excellent agreement is obtained. The obtained numerical results revealed the following concluding remarks:

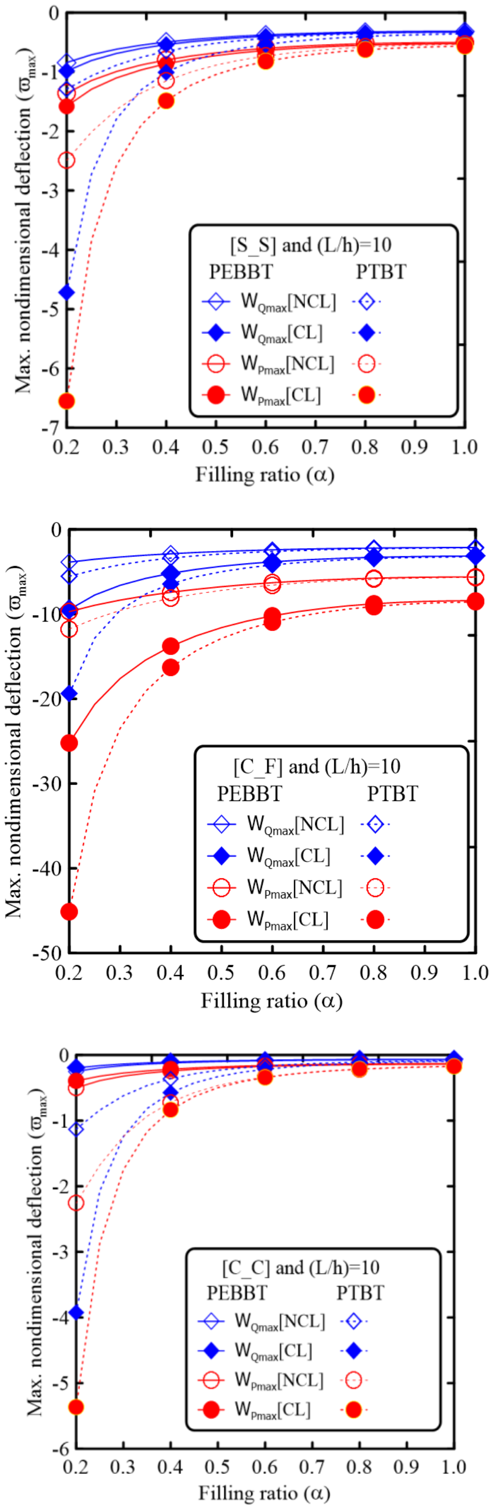

Fig. 4 Variation of the maximum nondimensional deflection with the filling ratio for both PEBBT and PTBT for different BCs at *L*/*H*=10

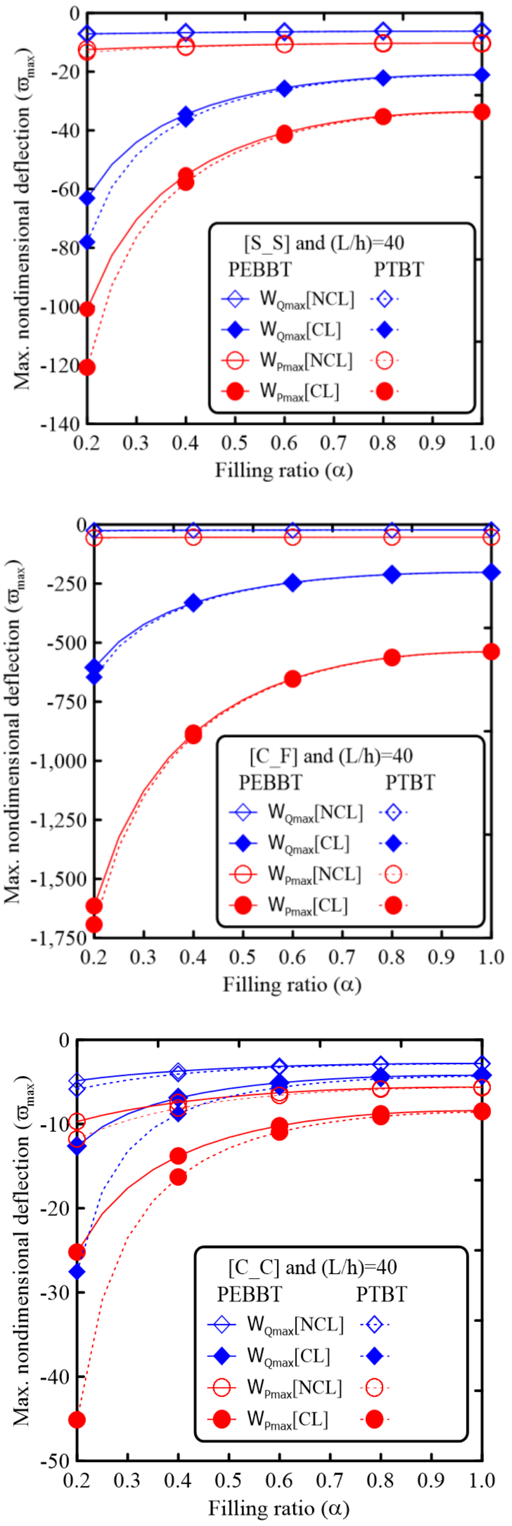

Fig. 5 Variation of the maximum nondimensional deflection with the filling ratio for both PEBBT and PTBT for different BCs at L/H=40

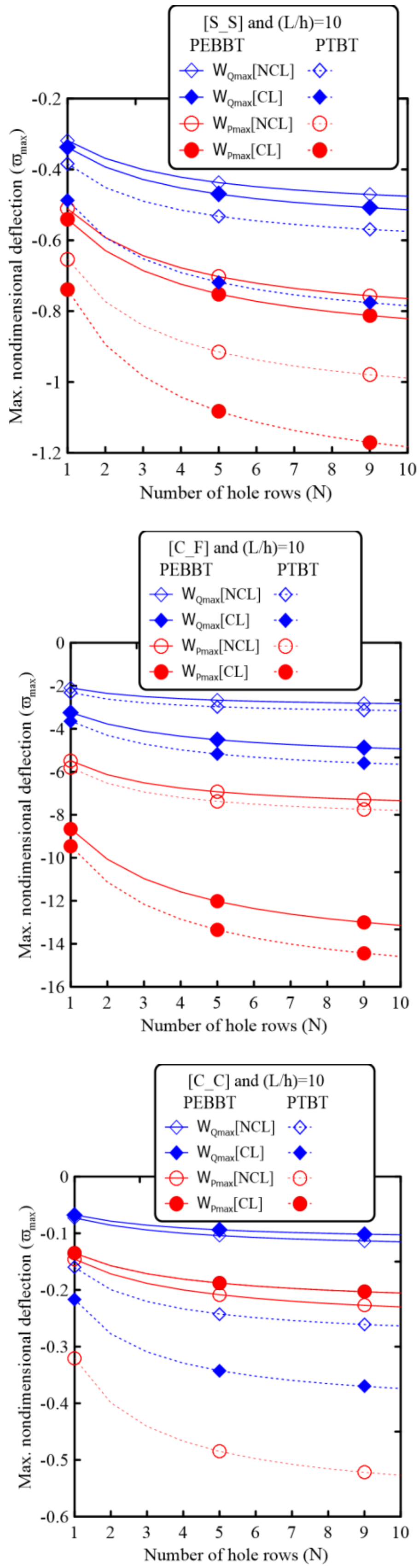

Fig. 6 Variation of the maximum nondimensional deflection with the number of hole rows for both PEBBT and PTBT for different BCs at *L/H*=10

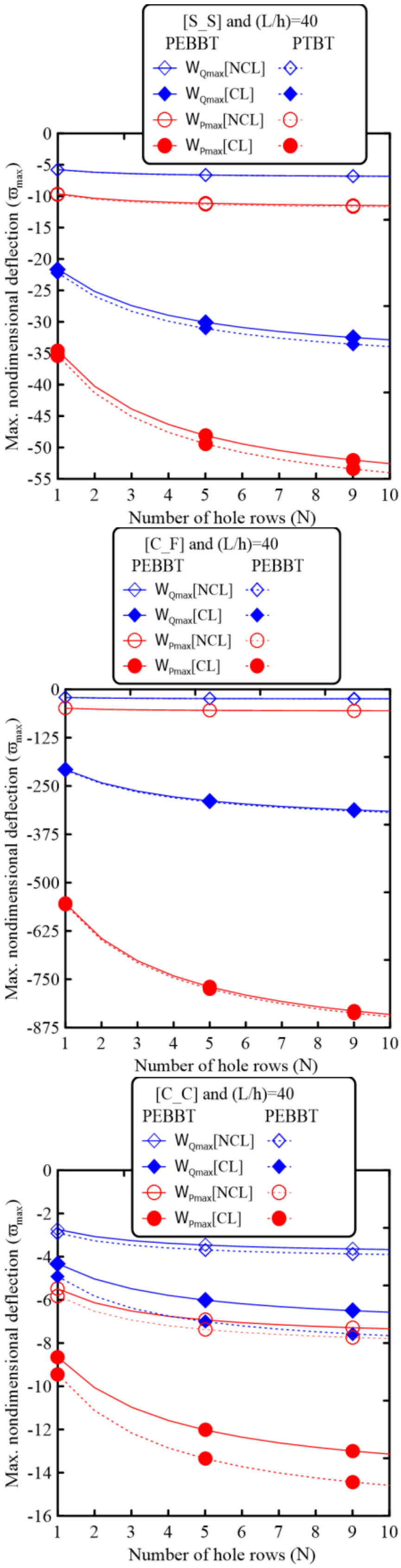

Fig. 7 Variation of the maximum nondimensional deflection with the number of hole rows for both PEBBT and PTBT for different BCs at *L/H*=40

- Surface stresses significantly effects on maximum bending deflection, this effect is mainly size dependent. The difference of the obtained results obtained based on the nonclassical surface elasticity model and the corresponding results based on classical models relies on the magnitudes of the surface properties.
- An intrinsic length parameter controlled by both surface elastic properties and the nanobeam bulk material properties can be established to characterize the surface energy effects for beam bending. Increasing the perforated nanobeam aspect ratio results in increasing the difference between the classical and nonclassical values of bending deflection.
- The surface residual stress, τ_s has more significant effect on the bending deflection compared with the corresponding effect of the surface elasticity, E_s.
- As the number of holes throughout the cross section of the perforated nanobeams increases the maximum nondimensional bending deflection increases due to increasing the beam flexibility.
- The perforated nanobeams filling ratio significantly affects the bending behavior of perforated nanobeams. As the filling ratio increases the maximum nondimensional bending deflection decreases due to decreasing the beam flexibility.
- For perforated nanobeams with lower aspect ratio (L/h) the Euler Bernoulli beam theory can't effectively investigate the bending behavior of perforated nanobeams especially at lower values of filling ratio (α<0.5).
- The nonclassical boundary conditions significantly affect bending behaviors of perforated nanobeams. Although the perforated nanobeams aspect ratio reaches (L/h=40), a remarkable difference is detected between bending behaviors investigated based on PEBBT and the corresponding behaviors investigated based on PTBT for C_C boundary conditions especially at lower values of filling ratio.

Acknowledgments

This work was funded by the Deanship of Scientific Research (DSR), King Abdulaziz University, Jeddah, under grant No. (DF-096-135-1441). The authors, therefore, acknowledge with thanks DSR technical and financial support

References

Abdelrahman, A.A., Eltaher, M.A., Kabeel, A.M., Abdraboh, A. M. and Hendi, A.A. (2019), "Free and forced analysis of perforated beams", *Steel Compos. Struct.*, **31**(5), 489-502. https://doi.org/10.12989/scs.2019.31.5.489.

Agwa, M.A. and Eltaher, M.A. (2016), "Vibration of a carbyne nanomechanical mass sensor with surface effect", *Appl. Phys. A*, **122**(4), 335. https://doi.org/10.1007/s00339-016-9934-9.

Almitani, K.H., Abdelrahman, A.A. and Eltaher, M.A. (2019), "On forced and free vibrations of cutout squared beams", *Steel Compos. Struct.*, **32**(5), 643-655. https://doi.org/10.12989/scs.2019.32.5.643

Almitani, K.H., Abdelrahman, A.A. and Eltaher, M.A. (2020), "Stability of perforated nanobeams incorporating surface energy effects", *Steel Compos. Struct.*, **35**(4), 555-566. https://doi.org/10.12989/scs.2020.35.4.555

Alimirzaei, S., Mohammadimehr, M. and Tounsi, A. (2019), "Nonlinear analysis of viscoelastic micro-composite beam with geometrical imperfection using FEM: MSGT electro-magneto-elastic bending, buckling and vibration solutions", *Struct. Eng. Mech.*, **71**(5), 485-502. https://doi.org/10.12989/sem.2019.71.5.485.

Ansari, R. and Sahmani, S. (2011), "Bending behavior and buckling of nanobeams including surface stress effects corresponding to different beam theories", *Int. J. Eng. Sci.*, **49**(11), 1244-1255. https://doi.org/10.1016/j.ijengsci.2011.01.007.

Ansari, R., Torabi, J. and Hassani, R. (2019), "Vibration analysis of FG-CNTRC plates with an arbitrarily shaped cutout based on the variational differential quadrature finite element method", *Mater. Res. Express*, **6**(12), 125086. https://doi.org/10.1088/2053-1591/ab5b57.

Ansari, R., Hassani, R. and Torabi, J. (2020), "Mixed-type formulation of higher-order shear deformation theory for vibration and buckling analysis of FG-GPLRC plates using VDQFEM", *Compos. Struct.*, **235**, 111738.https://doi.org/10.1016/j.compstruct.2019.111738

Asghar, S., Naeem, M.N., Hussain, M., Taj, M. and Tounsi, A. (2020), "Prediction and assessment of nonlocal natural frequencies of DWCNTs: Vibration analysis", *Comput. Concrete*, **25**(2), 133-144. https://doi.org/10.12989/cac.2020.25.2.133.

Balubaid, M., Tounsi, A., Dakhel, B. and Mahmoud, S.R. (2019), "Free vibration investigation of FG nanoscale plate using nonlocal two variables integral refined plate theory", *Comput. Concrete*, **24**(6), 579-586. https://doi.org/10.12989/cac.2019.24.6.579.

Barretta, R. and de Sciarra, F.M. (2018), "Constitutive boundary conditions for nonlocal strain gradient elastic nano-beams", *Int. J. Eng. Sci.*, **130**, 187-198. https://doi.org/10.1016/j.ijengsci.2018.05.009.

Barretta, R., Caporale, A., Faghidian, S.A., Luciano, R., de Sciarra, F.M. and Medaglia, C.M. (2019), "A stress-driven local-nonlocal mixture model for Timoshenko nano-beams", *Compos. Part B: Eng.*, **164**, 590-598. https://doi.org/10.1016/j.compositesb.2019.01.012.

Bedia, W.A., Houari, M.S.A., Bessaim, A., Bousahla, A.A., Tounsi, A., Saeed, T. and Alhodaly, M.S. (2019), "A new hyperbolic two-unknown beam model for bending and buckling analysis of a nonlocal strain gradient nanobeams", *J. Nano Res.*, **57**, 175-191. Trans Tech Publications Ltd. DOI: https://doi.org/10.12989/anr.2019.7.2.089

Bellal, M., Hebali, H., Heireche, H., Bousahla, A.A., Tounsi, A., Bourada, F. and Tounsi, A. (2020), "Buckling behavior of a single-layered graphene sheet resting on viscoelastic medium via nonlocal four-unknown integral model", *Steel Compos. Struct.*, **34**(5), 643-655. https://doi.org/10.12989/scs.2020.34.5.643.

Bellifa, H., Benrahou, K.H., Bousahla, A.A., Tounsi, A. and Mahmoud, S.R. (2017), "A nonlocal zeroth-order shear deformation theory for nonlinear postbuckling of nanobeams", *Struct. Eng. Mech.*, **62**(6), 695-702. https://doi.org/10.12989/sem.2017.62.6.695

Benahmed, A., Fahsi, B., Benzair, A., Zidour, M., Bourada, F. and Tounsi, A. (2019), "Critical buckling of functionally graded nanoscale beam with porosities using nonlocal higher-order shear deformation", *Struct. Eng. Mech.*, **69**(4), 457-466. https://doi.org/10.12989/sem.2019.69.4.457.

Berghouti, H., Adda Bedia, E.A., Benkhedda, A. and Tounsi, A. (2019), "Vibration analysis of nonlocal porous nanobeams made of functionally graded material", *Adv. Nano Res*, **7**(5), 351-364. https://doi.org/10.12989/anr.2019.7.5.351.

Bousahla, A.A., Bourada, F., Mahmoud, S.R., Tounsi, A., Algarni, A., Bedia, E.A. and Tounsi, A. (2020), "Buckling and dynamic behavior of the simply supported CNT-RC beams using an integral-first shear deformation theory", *Comput. Concrete*, **25**(2), 155-166. https://doi.org/10.12989/cac.2020.25.2.155.

Boutaleb, S., Benrahou, K. H., Bakora, A., Algarni, A., Bousahla, A.A., Tounsi, A. and Mahmoud, S.R. (2019), "Dynamic analysis of nanosize FG rectangular plates based on simple nonlocal quasi 3D HSDT", *Adv. Nano Res.*, **7**(3), 191-208. https://doi.org/10.12989/anr.2019.7.3.191.

Bourouina, H., Yahiaoui, R., Sahar, A. and Benamar, M.E.A. (2016), "Analytical modeling for the determination of nonlocal resonance frequencies of perforated nanobeams subjected to temperature-induced loads", *Physica E*, **75**, 163-168. https://doi.org/10.1016/j.physe.2015.09.014.

Chaabane, L.A., Bourada, F., Sekkal, M., Zerouati, S., Zaoui, F.Z., Tounsi, A. and Tounsi, A. (2019), "Analytical study of bending and free vibration responses of functionally graded beams resting on elastic foundation", *Struct. Eng. Mech.*, **71**(2), 185-196. https://doi.org/10.12989/sem.2019.71.2.185.

Chan, J., Eichenfield, M., Camacho, R. and Painter, O. (2009), "Optical and mechanical design of a "zipper" photonic crystal optomechanical cavity", *Optics Express*, **17**(5), 3802-3817. https://doi.org/10.1364/OE.17.003802.

Choudhary, P.K., Mahato, P.K. and Jana, P. (2019), "Optimal location of cutout within a cross-ply laminated cantilever beam for maximum lateral buckling load", *J. Physics: Conference Series* (Vol. 1240, No. 1, p. 012084). IOP Publishing., https://doi.org/10.1088/1742-6596/1240/1/012084.

Ebrahimi, F., Daman, M. and Fardshad, R.E. (2017), "Surface effects on vibration and buckling behavior of embedded nanoarches", *Struct. Eng. Mech.*, **64**(1), 1-10. https://doi.org/10.12989/sem.2017.64.1.001.

Ebrahimi, F. and Barati, M.R. (2018), "Surface and flexoelectricity effects on size-dependent thermal stability analysis of smart piezoelectric nanoplates", *Struct. Eng. Mech.*, **67**(2), 143-153. https://doi.org/10.12989/sem.2018.67.2.143.

Ebrahimi, F. and Barati, M.R. (2018), "Stability analysis of porous multi-phase nanocrystalline nonlocal beams based on a general higher-order couple-stress beam model", *Struct. Eng. Mech.*, **65**(4), 465-476. https://doi.org/10.12989/sem.2018.65.4.465.

Ebrahimi, F., Jafari, A. and Mahesh, V. (2019a), "Assessment of porosity influence on dynamic characteristics of smart heterogeneous magneto-electro-elastic plates", *Struct. Eng. Mech.*, **72**(1), 113-129. https://doi.org/10.12989/sem.2019.72.1.113

Ebrahimi, F., Fardshad, R.E. and Mahesh, V. (2019b), "Frequency response analysis of curved embedded magneto-electro-viscoelastic functionally graded nanobeams", *Adv. Nano Res.*, **7**(6), 391. https://doi.org/10.12989/anr.2019.7.6.391.

Ebrahimi, F., Karimiasl, M., Civalek, Ö. and Vinyas, M. (2019c), "Surface effects on scale-dependent vibration behavior of flexoelectric sandwich nanobeams", *Adv. Nano Res.*, **7**(2), 77. https://doi.org/10.12989/anr.2019.7.2.077.

Ebrahimi, F., Karimiasl, M. and Mahesh, V. (2019d), "Vibration analysis of magneto-flexo-electrically actuated porous rotary nanobeams considering thermal effects via nonlocal strain gradient elasticity theory", *Adv. Nano Res.*, **7**(4), 223-231. https://doi.org/10.12989/anr.2019.7.4.223.

Ebrahimi, F., Farazmandnia, N., Kokaba, M.R. and Mahesh, V. (2019e), "Vibration analysis of porous magneto-electro-elastically actuated carbon nanotube-reinforced composite sandwich plate based on a refined plate theory", *Eng.with Comput.*, 1-16. https://doi.org/10.1007/s00366-019-00864-4.

Eltaher, M.A., Mahmoud, F.F., Assie, A.E. and Meletis, E.I. (2013a), "Coupling effects of nonlocal and surface energy on vibration analysis of nanobeams", *Appl. Math. Comput.*, **224**, 760-774. https://doi.org/10.1016/j.amc.2013.09.002.

Eltaher, M.A., Hamed, M.A., Sadoun, A.M., and Mansour, A. (2014a), "Mechanical analysis of higher order gradient nanobeams", *Appl. Math. Comput.*, **229**, 260-272. https://doi.org/10.1016/j.amc.2013.12.076.

Eltaher, M.A., El-Borgi, S. and Reddy, J.N. (2016), "Nonlinear analysis of size-dependent and material-dependent nonlocal CNTs", *Compos. Struct.*, **153**, 902-913. https://doi.org/10.1016/j.compstruct.2016.07.013.

Eltaher, M.A., Kabeel, A.M., Almitani, K.H. and Abdraboh, A.M. (2018a), "Static bending and buckling of perforated nonlocal size-dependent nanobeams", *Microsystem Technologies*, **24**(12), 4881-4893. https://doi.org/10.1007/s00542-018-3905-3.

Eltaher, M.A., Abdraboh, A.M. and Almitani, K.H. (2018b), "Resonance frequencies of size dependent perforated nonlocal nanobeam", *Microsystem Technologies*, **24**(9), 3925-3937. https://doi.org/10.1007/s00542-018-3910-6.

Eltaher, M.A., Omar, F.A., Abdalla, W.S. and Gad, E.H. (2019a), "Bending and vibrational behaviors of piezoelectric nonlocal nanobeam including surface elasticity", *Waves in Random and Complex Media*, **29**(2), 264-280. https://doi.org/10.1080/17455030.2018.1429693.

Eltaher, M.A., Omar, F.A., Abdraboh, A.M., Abdalla, W.S., and A.E. Alshorbagy. (2020a), "Mechanical Behaviors of Piezoelectric Nonlocal Nanobeam with Cutouts", *Smart Structures and Systems*, **25**(2), 219-228. https://doi.org/10.12989/sss.2020.25.2.219.

Eltaher, M.A., Omar, F.A., Abdalla, W.S., Kabeel, M.A. and Alshorbagy, A.E. (2020b), "Mechanical analysis of cutout piezoelectric nonlocal nanobeam including surface energy effects", *Structural Engineering and Mechanics.*

Eltaher, M.A. and Mohamed, N. (2020a), "Nonlinear Stability and Vibration of Imperfect CNTs by Doublet Mechanics", *Appl. Math. Comput.*, **382**, 125311. https://doi.org/10.1016/j.amc.2020.125311.

Eltaher, M.A. and Mohamed, N.A. (2020b), "Vibration of Nonlocal Perforated Nanobeams under General Boundary Conditions", *Smart Struct. Syst.*, **25**(4), 510-514. https://doi.org/10.12989/sss.2020.25.4.501.

Gurtin, M.E. and Murdoch, A.I. (1975), "A continuum theory of elastic material surfaces", *Archive for Rational Mech. Ana.*, **57**(4), 291-323.

Gurtin, M.E. and Murdoch, A.I. (1978), "Surface stress in solids", *Int. J. Solids Struct.*, **14**(6), 431-440.

Hamed, M.A., Sadoun, A.M. and Eltaher, M.A. (2019), "Effects of porosity models on static behavior of size dependent functionally graded beam", *Struct. Eng. Mech.*, **71**(1), 89-98. https://doi.org/10.12989/sem.2019.71.1.089.

Hamed, M.A., Mohamed, N. and Eltaher, M.A. (2020), "Stability Buckling and Bending of Nanobeams including Cutouts", *Eng. with Comput.*, **1-14**. https://doi.org/10.1007/s00366-020-01063-2.

Hussain, M., Naeem, M.N., Tounsi, A. and Taj, M. (2019), "Nonlocal effect on the vibration of armchair and zigzag SWCNTs with bending rigidity", *Adv. Nano Res.*, **7**(6), 431-442. https://doi.org/10.12989/anr.2019.7.6.431.

Hussain, M., Naeem, M.N., Taj, M. and Tounsi, A. (2020), "Simulating vibration of single-walled carbon nanotube using Rayleigh-Ritz's method", *Adv. Nano Res.*, **8**(3), 215-228. https://doi.org/10.12989/anr.2020.8.3.215.

Jeong, K.H. and Amabili, M. (2006), "Bending vibration of perforated beams in contact with a liquid", *J. Sound Vib.*, **298**(1-2), 404-419. https://doi.org/10.1016/j.jsv.2006.05.029.

Karami, B., Janghorban, M. and Tounsi, A. (2019), "Galerkin's approach for buckling analysis of functionally graded anisotropic nanoplates/different boundary conditions", *Eng. with Comput.*, **35**(4), 1297-1316. https://doi.org/10.1007/s00366-018-0664-9

Karami, B., Janghorban, M. and Tounsi, A. (2019), "On pre-stressed functionally graded anisotropic nanoshell in magnetic field", *J. Braz. Soc. Mech. Sci. Eng.*, **41**(11), 495. https://doi.org/10.1007/s40430-019-1996-0.

Karimiasl, M., Ebrahimi, F. and Mahesh, V. (2019a), "Nonlinear forced vibration of smart multiscale sandwich composite doubly curved porous shell", *Thin-Wall. Struct.*, **143**, 106152. https://doi.org/10.1016/j.tws.2019.04.044.

Karimiasl, M., Ebrahimi, F. and Mahesh, V. (2019b), "Postbuckling analysis of piezoelectric multiscale sandwich composite doubly curved porous shallow shells via Homotopy Perturbation Method", *Eng. with Comput.*, 1-17. https://doi.org/10.1007/s00366-019-00841-x.

Kerid, R., Bourouina, H., Yahiaoui, R., Bounekhla, M. and Aissat, A. (2019), "Magnetic field effect on nonlocal resonance frequencies of structure-based filter with periodic square holes network", *Physica E: Low-dimensional Syst. Nanostruct.*, **105**, 83-89. https://doi.org/10.1016/j.physe.2018.05.021.

Khater, M.E., Eltaher, M.A., Abdel-Rahman, E. and Yavuz, M. (2014), "Surface and thermal load effects on the buckling of curved nanowires", *Eng. Sci. Technol.*, **17**(4), 279-283. https://doi.org/10.1016/j.jestch.2014.07.003.

Khatir, S., Tiachacht, S., Thanh, C.L., Bui, T.Q. and Wahab, M.A. (2019), "Damage assessment in composite laminates using ANN-PSO-IGA and Cornwell indicator", *Compos. Struct.*, **230**, 111509. https://doi.org/10.1016/j.compstruct.2019.111509.

Kim, J.H., Jeon, J.H., Park, J.S., Seo, H.D., Ahn, H.J. and Lee, J. M. (2015), "Effect of reinforcement on buckling and ultimate strength of perforated plates", *Int. J. Mech. Sci.*, **92**, 194-205. https://doi.org/10.1016/j.ijmecsci.2014.12.016.

Li, L., Tang, H. and Hu, Y. (2018), "The effect of thickness on the mechanics of nanobeams", *Int. J. Eng. Sci.*, **123**, 81-91. https://doi.org/10.1016/j.ijengsci.2017.11.021.

Liu, C. and Rajapakse, R.K.N.D. (2009), "Continuum models incorporating surface energy for static and dynamic response of nanoscale beams", *IEEE T. Nanotechnology*, **9**(4), 422-431. 10.1109/TNANO.2009.2034142.

Luschi, L. and Pieri, F. (2012), "A simple analytical model for the resonance frequency of perforated beams", *Procedia Eng.*, **47**, 1093-1096. https://doi.org/10.1016/j.proeng.2012.09.341.

Luschi, L. and Pieri, F. (2014), "An analytical model for the determination of resonance frequencies of perforated beams", *J. Micromech. Microeng.*, **24**(5), 055004. https://doi.org/10.1088/0960-1317/24/5/055004.

Luschi, L. and Pieri, F. (2016), "An analytical model for the resonance frequency of square perforated Lamé-mode resonators", *Sensor. Actuators B: Chemical*, **222**, 1233-1239. https://doi.org/10.1016/j.snb.2015.07.085.

Mahesh, V., Kattimani, S., Harursampath, D. and Trung, N.T. (2019), "Coupled evaluation of the free vibration characteristics of magneto-electro-elastic skew plates in hygrothermal environment", *Smart Struct. Syst.*, **24**(2), 267-292. https://doi.org/10.12989/sss.2019.24.2.267.

Mahesh, V., Sagar, P.J. and Kattimani, S. (2018), "Influence of coupled fields on free vibration and static behavior of functionally graded magneto-electro-thermo-elastic plate", *J. Intel. Mat. Syst. Str.*, **29**(7), 1430-1455. https://doi.org/10.1177/1045389X17740739.

Mahmoud, F.F., Eltaher, M.A., Alshorbagy, A.E. and Meletis, E.I. (2012), "Static analysis of nanobeams including surface effects by nonlocal finite element", *J. Mech. Sci. Technol.*, **26**(11), 3555-3563. DOI 10.1007/s12206-012-0871-z.

Miller, R.E. and Shenoy, V.B. (2000), "Size-dependent elastic properties of nanosized structural elements", *Nanotechnology*, **11**(3), 139. https://doi.org/10.1088/0957-4484/11/3/301.

Mohamed, N., Eltaher, M.A., Mohamed, S.A. and Seddek, L.F. (2019), "Energy equivalent model in analysis of postbuckling of imperfect carbon nanotubes resting on nonlinear elastic foundation", *Struct. Eng. Mech.*, **70**(6), 737-750. https://doi.org/10.12989/sem.2019.70.6.737.

Mohamed, N., Mohamed, S.A. and Eltaher, M.A. (2020), "Buckling and post-buckling behaviors of higher order carbon nanotubes using energy-equivalent model", *Eng. with Comput.*, 1-14. https://doi.org/10.1007/s00366-020-00976-2.

Phung-Van, P., Tran, L.V., Ferreira, A.J.M., Nguyen-Xuan, H. and Abdel-Wahab, M. (2017a), "Nonlinear transient isogeometric analysis of smart piezoelectric functionally graded material plates based on generalized shear deformation theory under thermo-electro-mechanical loads", *Nonlinear Dynam.*, **8**7(2), 879-894. https://doi.org/10.1007/s11071-016-3085-6.

Phung-Van, P., Ferreira, A.J.M., Nguyen-Xuan, H. and Wahab, M. A. (2017b), "An isogeometric approach for size-dependent geometrically nonlinear transient analysis of functionally graded nanoplates", *Compos. Part B: Eng.*, **118**, 125-134. https://doi.org/10.1016/j.compositesb.2017.03.012.

Phung-Van, P., Thanh, C.L., Nguyen-Xuan, H. and Abdel-Wahab, M. (2018), "Nonlinear transient isogeometric analysis of FG-CNTRC nanoplates in thermal environments", *Compos. Struct.*, **201**, 882-892. https://doi.org/10.1016/j.compstruct.2018.06.087.

Phung-Van, P., Thai, C.H., Nguyen-Xuan, H. and Wahab, M.A. (2019), "Porosity-dependent nonlinear transient responses of functionally graded nanoplates using isogeometric analysis", *Compos. Part B: Eng.*, **164**, 215-225. https://doi.org/10.1016/j.compositesb.2018.11.036.

Romano, G., Barretta, R., Diaco, M. and de Sciarra, F.M. (2017), "Constitutive boundary conditions and paradoxes in nonlocal elastic nanobeams", *Int. J. Mech. Sci.*, **121**, 151-156. https://doi.org/10.1016/j.ijmecsci.2016.10.036.

Semmah, A., Heireche, H., Bousahla, A.A. and Tounsi, A. (2019), "Thermal buckling analysis of SWBNNT on Winkler foundation by non local FSDT", *Adv. Nano Res.*, **7**(2), 89-98. https://doi.org/10.12989/anr.2019.7.2.089.

Shariati, A., Habibi, M., Tounsi, A., Safarpour, H. and Safa, M. (2020), "Application of exact continuum size-dependent theory for stability and frequency analysis of a curved cantilevered microtubule by considering viscoelastic properties". *Eng. with Comput.*, https://doi.org/10.1007/s00366-020-01024-9.

Sivakumar, N., Kanagasabapathy, H. and Srikanth, H.P. (2018), "Analysis of Perforated Piezoelectric Sandwich Smart Structure Cantilever Beam Using COMSOL", *Materials Today: Proceedings*, **5**(5), 12025-12034. https://doi.org/10.1016/j.matpr.2018.02.177.

Sun, F., Wang, P., Li, W., Fan, H. and Fang, D. (2017), "Effects of circular cutouts on mechanical behaviors of carbon fiber reinforced lattice-core sandwich cylinder", *Compos. Part A: Appl. Sci. Manufact.*, **100**, 313-323. https://doi.org/10.1016/j.compositesa.2017.05.029.

Taj, M., Majeed, A., Hussain, M., Naeem, M.N., Safeer, M., Ahmad, M. and Tounsi, A. (2020), "Non-local orthotropic elastic shell model for vibration analysis of protein microtubules", *Comput. Concrete*, **25**(3), 245-253. https://doi.org/10.12989/cac.2020.25.3.245.

Tlidji, Y., Zidour, M., Draiche, K., Safa, A., Bourada, M., Tounsi, A. and Mahmoud, S.R. (2019), "Vibration analysis of different material distributions of functionally graded microbeam", *Struct. Eng. Mech.*, **69**(6), 637-649. https://doi.org/10.12989/sem.2019.69.6.637.

Thanh, C.L., Phung-Van, P., Thai, C.H., Nguyen-Xuan, H. and Wahab, M.A. (2018), "Isogeometric analysis of functionally graded carbon nanotube reinforced composite nanoplates using modified couple stress theory", *Compos. Struct.*, **184**, 633-649. https://doi.org/10.1016/j.compstruct.2017.10.025.

Thanh, C.L., Tran, L.V., Vu-Huu, T., Nguyen-Xuan, H. and Abdel-Wahab, M. (2019a), "Size-dependent nonlinear analysis and damping responses of FG-CNTRC micro-plates", *Comput. Method. Appl. M.*, **353**, 253-276. https://doi.org/10.1016/j.cma.2019.05.002.

Thanh, C.L., Tran, L.V., Bui, T.Q., Nguyen, H.X. and Abdel-Wahab, M. (2019b), "Isogeometric analysis for size-dependent nonlinear thermal stability of porous FG microplates", *Compos. Struct.*, **221**, 110838. https://doi.org/10.1016/j.compstruct.2019.04.010.

Thanh, C.L., Ferreira, A.J.M. and Wahab, M.A. (2019c), "A refined size-dependent couple stress theory for laminated composite micro-plates using isogeometric analysis", *Thin-Wall. Struct.*, **145**, 106427. https://doi.org/10.1016/j.tws.2019.106427.

Thanh, C.L., Tran, L.V., Vu-Huu, T. and Abdel-Wahab, M. (2019d), "The size-dependent thermal bending and buckling analyses of composite laminate microplate based on new modified couple stress theory and isogeometric analysis", *Comput. Method. Appl. M.*, **350**, 337-361. https://doi.org/10.1016/j.cma.2019.02.028.

Vinyas, M. (2020a), "Computational Analysis of Smart Magneto-Electro-Elastic Materials and Structures: Review and Classification", *Archiv. Comput. Method. Eng.*, 1-44. https://doi.org/10.1007/s11831-020-09406-4.

Vinyas, M. (2020b)," Interphase effect on the controlled frequency response of three-phase smart magneto-electro-elastic plates embedded with active constrained layer damping: FE study", *Mater. Res. Express*, **6**(12), 125707. https://doi.org/10.1088/2053-1591/ab6649.

Vinyas, M. (2020), "On frequency response of porous functionally graded magneto-electro-elastic circular and annular plates with different electro-magnetic conditions using HSDT", *Compos. Struct.*, **240**, 112044. https://doi.org/10.1016/j.compstruct.2020.112044.

Vinyas, M. and Kattimani, S.C. (2017a), "A finite element based assessment of static behavior of multiphase magneto-electro-elastic beams under different thermal loading", *Struct. Eng. Mech.*, **62**(5), 519-535. https://doi.org/10.12989/sem.2017.62.5.519.

Vinyas, M. and Kattimani, S.C. (2017b), "Hygrothermal analysis of magneto-electro-elastic plate using 3D finite element analysis", *Compos. Struct.*, **18**0, 617-637. https://doi.org/10.1016/j.compstruct.2017.08.015.

Vinyas, M. and Kattimani, S.C. (2017c), "Static analysis of stepped functionally graded magneto-electro-elastic plates in thermal environment: a finite element study", *Compos. Struct.*, **178**, 63-86. https://doi.org/10.1016/j.compstruct.2017.06.068.

Vinyas, M. and Kattimani, S.C. (2017d), "Static behavior of thermally loaded multilayered Magneto-Electro-Elastic beam", *Struct. Eng. Mech.*, **63**(4), 481-495. https://doi.org/10.12989/sem.2017.63.4.481.

Vinyas, M. and Kattimani, S.C. (2017e), "Static studies of stepped functionally graded magneto-electro-elastic beam subjected to different thermal loads", *Compos. Struct.*, **163**, 216-237. https://doi.org/10.1016/j.compstruct.2016.12.040.

Vinyas, M. and Kattimani, S.C. (2018a), "Finite element evaluation of free vibration characteristics of magneto-electro-elastic rectangular plates in hygrothermal environment using higher-order shear deformation theory", *Compos. Struct.*, **202**, 1339-1352. https://doi.org/10.1016/j.compstruct.2018.06.069.

Vinyas, M. and Kattimani, S.C. (2018b), "Investigation of the effect of BaTiO3/CoFe2O4 particle arrangement on the static response of magneto-electro-thermo-elastic plates", *Compos. Struct.*, **185**, 51-64. https://doi.org/10.1016/j.compstruct.2017.10.073.

Vinyas, M., Kattimani, S.C. and Joladarashi, S. (2018a), "Hygrothermal coupling analysis of magneto-electroelastic beams using finite element methods", *J. Therm. Stresses*, **41**(8), 1063-1079. https://doi.org/10.1080/01495739.2018.1447856.

Vinyas, M., Kattimani, S.C., Loja, M.A.R. and Vishwas, M. (2018b), "Effect of BaTiO3/CoFe2O4 micro-topological textures on the coupled static behaviour of magneto-electro-thermo-elastic beams in different thermal environment", *Mater. Res. E*xpress, **5**(12), 125702. https://doi.org/10.1088/2053-1591/aae0c8.

Vinyas, M., Harursampath, D. and Kattimani, S.C. (2020a), "On vibration analysis of functionally graded carbon nanotube reinforced magneto-electro-elastic plates with different electro-magnetic conditions using higher order finite element methods", *Defence Technology*, articles in press. https://doi.org/10.1016/j.dt.2020.03.012.

Vinyas, M., Harursampath, D. and Thoi, T.N. (2020b), "A higher order coupled frequency characteristics study of smart magneto-electro-elastic composite plates with cut-outs using finite element methods", *Defence Technology*, articles in press. https://doi.org/10.1016/j.dt.2020.02.009.

Mahesh, V. and Kattimani, S. (2019), "Finite element simulation of controlled frequency response of skew multiphase magneto-electro-elastic plates", *J. Intel. Mater. Syst. Struct.*, **30**(12), 1757-1771. https://doi.org/10.1177/1045389X19843674.

Vinyas, M., Harursampath, D. and Nguyen-Thoi, T. (2019), "Influence of active constrained layer damping on the coupled vibration response of functionally graded magneto-electro-elastic plates with skewed edges". Defence Technology, articles in press. https://doi.org/10.1016/j.dt.2019.11.016.

Vinyas, M., Nischith, G., Loja, M.A.R., Ebrahimi, F. and Duc, N. D. (2019a), "Numerical analysis of the vibration response of skew magneto-electro-elastic plates based on the higher-order shear deformation theory", *Compos. Struct.*, **214**, 132-142. https://doi.org/10.1016/j.compstruct.2019.02.010.

Vinyas, M., Sandeep, A.S., Nguyen-Thoi, T., Ebrahimi, F. and Duc, D.N. (2019b), "A finite element–based assessment of free vibration behaviour of circular and annular magneto-electro-elastic plates using higher order shear deformation theory", *J. Intel. Mat. Syst. Str.*, **30**(16), 2478-2501. https://doi.org/10.1177/1045389X19862386.

Wang, G.F. and Feng, X.Q. (2007), "Effects of surface elasticity and residual surface tension on the natural frequency of microbeams", *Appl. Phys. Lett.*, **90**(23), 231904. https://doi.org/10.1063/1.2746950.

Xiao, Y., Wen, J. and Wen, X. (2012), "Broadband locally resonant beams containing multiple periodic arrays of attached resonators", *Phys. Lett. A*, **376**(16), 1384-1390. https://doi.org/10.1016/j.physleta.2012.02.059.

Yang, F.A.C.M., Chong, A.C.M., Lam, D.C.C. and Tong, P. (2002), "Couple stress-based strain gradient theory for elasticity", *Int. J. Solids Struct.*, **39**(10), 2731-2743. https://doi.org/10.1016/S0020-7683(02)00152-X.

Zhang, Z.J., Zhang, Q.C., Li, F.C., Yang, J.W., Liu, J.W., Liu, Z. Y. and Jin, F. (2019), "Modal characteristics of micro-perforated sandwich beams with square honeycomb-corrugation hybrid cores: A mixed experimental-numerical study", *Thin-Walle. Struct.*, **137**, 185-196. https://doi.org/10.1016/j.tws.2019.01.004 .

CC